KINETIC AND STRUCTURAL EFFECTS OF INTERFACIAL INTERRUPTION AND PROTEIN NITRATION IN HUMAN MANGANESE SUPEROXIDE DISMUTASE

By

PATRICK QUINT

A DISSERTATION PRESENTED TO THE GRADUATE SCHOOL
OF THE UNIVERSITY OF FLORIDA IN PARTIAL FULFILLMENT
OF THE REQUIREMENTS FOR THE DEGREE OF
DOCTOR OF PHILOSOPHY

UNIVERSITY OF FLORIDA

2006

ACKNOWLEDGMENTS

Sincere thanks go to my parents, brothers and sisters, and all those with whom I have shared the joy and frustration of this work. However, this dissertation would not have been possible without the patient encouragement of my wife Ingvild, the impish smile of my son Anders or the expert mentorship of Drs. Silverman and McKenna.

TABLE OF CONTENTS

page

LIST OF TABLES

LIST OF FIGURES

Abstract of Dissertation Presented to the Graduate School
of the University of Florida in Partial Fulfillment of the
Requirements for the Degree of Doctor of Philosophy

KINETIC AND STRUCTURAL EFFECTS OF INTERFACIAL INTERRUPTION AND PROTEIN NITRATION IN HUMAN MANGANESE SUPEROXIDE DISMUTASE

By

Patrick Quint

August 2006

Chair: David Silverman
Major Department: Biochemistry and Molecular Biology

This dissertation investigated interfacial attributes of human manganese superoxide dismutase (MnSOD), a homotetramer with two structurally unique interfaces. A conserved dimeric interface is formed from the junction of two subunits and the tetrameric interface is formed from the interaction of two dimer pairs. Using ^{19}F NMR, observation of chemical shift and linewidth changes for fluorine-labeled tyrosines in the dimeric and tetrameric interfaces of human MnSOD (Tyr169 and Tyr45 respectively) indicated greater rigidity in the dimeric interface compared to the tetrameric interface. Replacement of the dimeric, interfacial residue Glu162 with aspartate or alanine did not significantly alter the crystal structure of human MnSOD, though an interaction with a histidine ligand of the active site manganese was truncated. This interaction was mediated in E162D by an intervening solvent molecule. Catalytic activity for E162D and E162A was 5-20% that of wild-type enzyme and differential scanning calorimetry indicated a role for E162 in thermal stability. Nitration of Tyr34, a dimeric, interfacial residue involved in a hydrogen-bond network emanating from the active-site manganese, abolishes activity in human MnSOD. In vitro nitration of human MnSOD yielded 74%

nitration of Tyr34 with moderate nitration of other aromatic residues. A 2.4 Å structure of nitrated MnSOD aligned well with wild type though an NO_2 group covalently linked to Tyr34 is observed. The structure of nitro-MnSOD indicates that alteration of the hydrogen-bond network as well as steric blockade and electrostatic repulsion of substrate all account for the loss in catalytic activity associated with nitration. Taken together, these findings provide a role for the tetrameric interface in stability and the dimeric interface in catalysis. In addition, this dissertation provides a structural explanation for abolished catalytic activity associated with nitration of Tyr34 in MnSOD. Future therapeutic studies on this enzyme will involve the study of residues that form the dimeric interface of MnSOD.

CHAPTER 1
INTRODUCTION

Superoxide Formation and Reactions

Superoxide is an oxygen radical formed from the reaction of free electrons with O_2 to form $O_2^{\cdot -}$. There are several enzymatic sources of superoxide including xanthine oxidase, NADPH-oxidase within phagocytes, and other oxidases and an important endogenous source of superoxide are the mitochondria. Leaks in the electron transport chain allow for the addition of a single electron to O_2 to form $O_2^{\cdot -}$ (Kalra et al. 1994; Haliwell, 1995). Though superoxide is itself toxic to the cell, its primary mode of damage to cellular structures occurs through the Haber-Weiss reaction to form the highly unstable hydroxyl radical (Haber and Weiss, 1934). In addition, superoxide reacts with nitric oxide to form the nitrating agent peroxynitrite, which dissociates to form hydroxyl radical and nitrite radical (Beckman et al., 1990; Beckman et al., 1992). Superoxide and its breakdown products can cause damage to several biomolecules including lipids, DNA and proteins and can affect their normal function. Its reaction with proteins, lipids and DNA has implicated superoxide in several pathological states including reperfusion injury (Becker, 2004), degenerative diseases like amyotrophic lateral sclerosis and muscular dystrophy and has been implicated in damage induced aging of cells (Harman, 1956). To avoid the deleterious effects of the superoxide anion and hydroxyl radical, cells have evolved a mechanism to scavenge and catalyze the disproportionation of superoxide.

Classes of Superoxide Dismutase

Organisms that thrive in aerobic environments utilize superoxide dismutase (SOD) to scavenge and detoxify superoxide radicals. There are four isoforms of SOD that utilize for catalysis the metals copper and zinc, manganese, iron, and nickel. A copper containing protein with dismutase activity was first discovered in 1968 by McCord and Fridovich and a year later identified as a copper-containing SOD (McCord and Fridovich, 1968; McCord and Fridovich, 1969). The same group reported the discovery of a structurally unique SOD in *E. coli* that utilized manganese in its active site (Keele, McCord and Fridovich, 1970). It was later discovered that both Cu/ZnSOD and MnSOD are utilized by eukaryotes, though their localizations are different; Cu/ZnSOD is localized primarily in the cytosol while MnSOD is localized exclusively within the inner-mitochondrial matrix (Weisinger and Fridovich, 1973). Its localization in the mitochondrial matrix suggests a role for MnSOD in the protection of mitochondrial DNA, lipids and proteins. Eukaryotic organisms also express an extracellular SOD which utilizes copper and zinc for catalysis (Marklund, 1982). Like eukaryotic MnSOD, it is tetrameric in solution. Two other classes of SOD also exist: FeSOD, which is structurally similar to MnSOD with an identical active-site structure (Slykhouse and Fee, 1976) and the structurally unique NiSOD (Chodhury et al,. 1999; Barondeau et al., 2004).

Human Manganese Superoxide Dismutase

Active Site and Hydrogen Bond Network

Human manganese superoxide dismutase (MnSOD) is a homotetramer of 22 kDa subunits that catalyzes the disproportionation of superoxide into O_2 and H_2O_2 (Fridovich et al., 1989). Localized in the mitochondria, MnSOD is an enzyme with $k_{cat}/K_m = 8 \times 10^8$ M^{-1} sec^{-1} (Hsu et al., 1996). Structural studies done by Borgstahl et al. in 1992 reveal a

trigonal, bipyramidal geometry about the active site manganese composed of three histidines (His26, 74 and 163), one aspartate (Asp159) and one

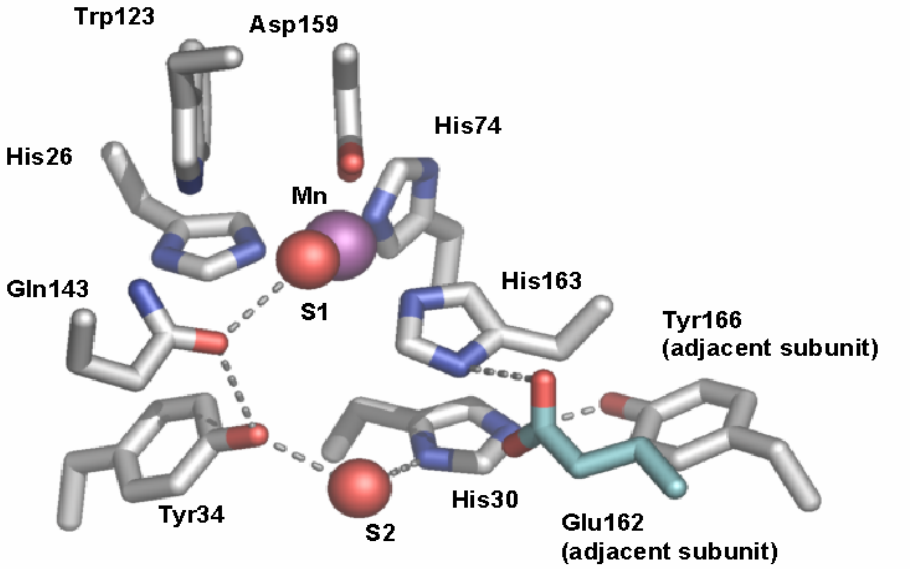

Figure 1-1 Hydrogen-bond network of human MnSOD. Shown in cyan are intervening residues from the adjacent, non-crystallographic subunit.

solvent molecule (Figure 1-1). A hydrogen bond network extends from the active site metal to the coordinating solvent molecule, through Gln143 to Tyr34, through a solvent to His30, and finally to Tyr166 from the adjacent subunit (Figure 1-1).

Manganese Superoxide Dismutase and its Reaction with Superoxide

Human MnSOD catalyzes the rapid disproportionation of superoxide through a two-step reaction in which the active-site manganese is first reduced and then oxidized with formation of products O_2 and H_2O_2 (see equation 1 and 2).

$$\mathbf{Mn(III)(OH)SOD + O_2^{\cdot -} + H^+ \xrightarrow{k1} Mn(II)(H_2O)SOD + O_2} \quad \mathbf{(1)}$$

$$\mathbf{Mn(II)(H_2O)SOD + O_2^{\cdot -} + H^+ \xrightarrow{k2} Mn(III)(OH)SOD + H_2O_2} \quad \mathbf{(2)}$$

$$\mathbf{Mn(II)(H_2O)SOD + O_2^{\cdot -} \xrightarrow{k3} Mn(III)(X)SOD} \quad \mathbf{(3)}$$

$$\mathbf{Mn(III)(X)SOD + H^+ + H_2O \xrightarrow{k4} Mn(III)(OH)SOD + H_2O_2} \quad \mathbf{(4)}$$

The scheme shown above indicates that the coordinated solvent of MnSOD is protonated upon reduction (Eq. 1) (Miller et al., 2003) and that one proton is donated from the coordinating solvent to form product H_2O_2 (Eq. 2). Catalysis is further complicated by the reversible formation and dissociation of a product inhibited complex, shown in equations 3 and 4 (McAdam et al., 1977; Bull et al., 1991). It is speculated that inhibition of the enzyme occurs through the oxidative addition of $O_2^{\cdot-}$ to Mn(II), shown in equation 3, forming a peroxo-bound complex of Mn(III) with the reverse of this reaction, shown in equation 4, yielding active enzyme (Bull et al., 1991).

The Subunit Interfaces of Human Manganese Superoxide Dismutase

Human MnSOD contains two interfaces, the dimeric interface, conserved between prokaryotes and eukaryotes, and the tetrameric interface generally associated with the eukaryotic enzyme (Figure 1-2) (Borgstahl et al., 1992). The dimeric interface is composed of several residues that participate in hydrogen bond interactions and the location of the hydrogen bond network (Fig 1-1 and Fig 1-2). The tetrameric interface is formed from the dimerization of dimers in the eukaryotic enzyme, creating a novel four-helix bundle, first described by Borgstahl et al. in 1992. The role of the tetrameric interface is unknown, though it likely plays a role in stabilizing the enzyme, thus providing an evolutionary advantage. The tetrameric interface does not appear to participate in catalysis. The scheme shown above indicates that the coordinating solvent of MnSOD is protonated upon reduction (Eq. 1) (Miller et al., 2003) and that one proton is donated from the coordinating solvent to form product H_2O_2 (Eq. 2).

Peroxynitrite

An important mechanism for catalytic inhibition is through the reaction of MnSOD with peroxynitrite. Peroxynitrite is a nitrating agent formed from the diffusion-controlled

reaction of superoxide with nitric oxide (Beckman et al., 1990). Upon protonation, peroxynitrite dissociates to form nitrate (70%) and hydroxyl and nitrite radicals (30%) with a first order rate constant of 0.17 sec^{-1} (Beckman et al., 1990). The reaction of hydroxyl radicals with biomolecules results in the one-electron oxidation of lipids, proteins and DNA. However, hydroxyl radical formation is likely to occur at acidic pH when peroxynitrite is in its protonated form, but at physiological pH its reaction with CO_2 becomes important. At pH 7.8, peroxynitrite reacts with CO_2 to form nitrosoperoxycarbonate and out competes the spontaneous dissociation of peroxynitrous acid (Bonini et al., 1999). The short-lived nitrosoperoxycarbonate intermediate dissociates into nitrate (~65%) and carbonate radicals (~35%) which mediate the formation of 3-nitrotyrosine.

Tyrosine Nitration

Electron paramagnetic resonance studies have shown that tyrosine nitration by peroxynitrite is increased in the presence of CO_2, and membrane inlet mass spectrometry studies have shown that CO_2 catalyzes the isomerization of peroxynitrite into nitrate through a nitrosoperoxycarbonate intermediate (Santos et al., 2000; Tu et al., 2004). The predominant pathway for tyrosine nitration is through the reaction of carbonate radical with tyrosine to form tyrosyl radical. Though hydroxyl radical is capable of forming tyrosyl radical, it is a more promiscuous oxidative agent than $CO_3^{\cdot -}$. It has been shown previously that catalytic inhibition of MnSOD results primarily from the nitration of Tyr34 (MacMillan-Crow et al., 1996; Yamakura et al., 2001). The mechanism for this substantial decrease has been elucidated by a 2.4 Å structure of nitrated human MnSOD indicating that steric hindrance or bulk blockade of the substrate access channel may be

responsible for the change in activity (Quint and Reutzel et al., 2005). These results are discussed in chapter 4.

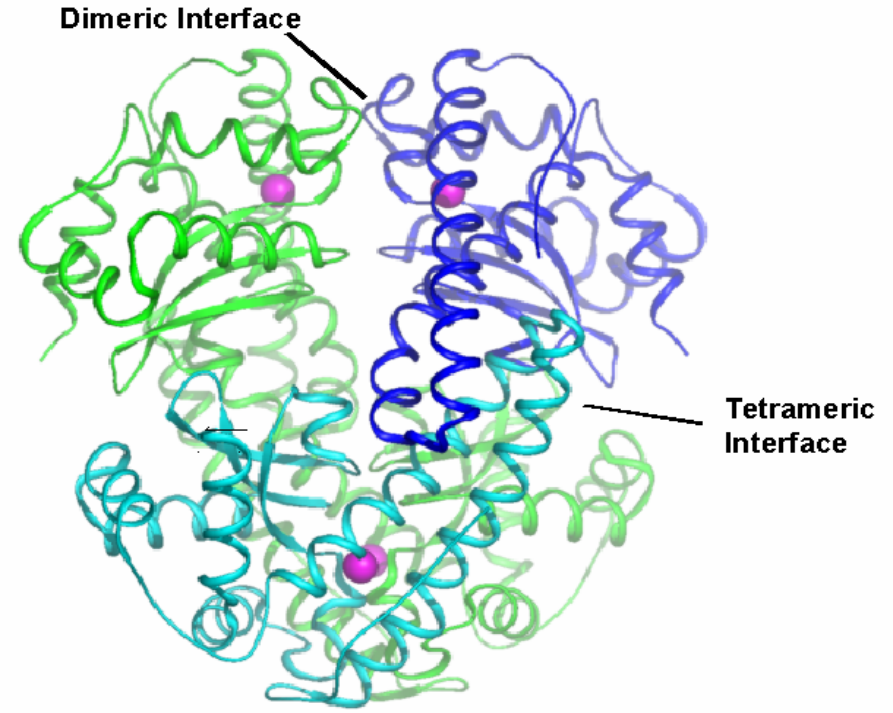

Figure 1-2 Tetrameric human MnSOD. The dimeric interface is shown in green and blue and the tetrameric interface is shown in blue and orange. Magenta spheres are active site manganese.

Research Goals

The data and conclusions presented in this thesis focus on the role of the subunit interfaces in human MnSOD and the structural effects of nitration of Tyr34. Techniques utilized include ^{19}F NMR, x-ray crystallography, differential scanning calorimetry, mass spectrometry, site-directed mutagenesis and pulse radiolysis. The first aim was to define the contribution of the two subunit interfaces to enzymatic stability. Building on the conclusions of the first study, the involvement of the dimeric interface in stability and catalysis was probed through replacement of Glu162. Finally, a structure of nitrated human MnSOD was determined.

Interfacial Mobility at the Dimeric and Tetrameric Interfaces of Human Manganese Superoxide Dismutase

The tetrameric interface is generally associated with eukaryotic enzymes. The advantage of a tetrameric structure over a dimeric structure in human MnSOD is not yet understood. The goal of this study was to understand differences in stability exhibited by the two structurally unique interfaces of human MnSOD. Using fluorine labeled Tyr169 as a reporter for the dimeric interface and fluorine labeled Tyr45 as a reporter for the tetrameric interface, ^{19}F NMR was utilized to probe the conformational mobility of the two interfaces. The data indicate that the dimeric interface is significantly less conformationally mobile than the tetrameric interface, suggesting a role for the tetrameric interface in thermal stability. This study will provide a better understanding of the role of both interfaces in stability and may aid in our understanding of the evolutionary role of the tetrameric interface.

Replacement of a Key Dimeric Interfacial Residue

Following the thermostability work of the previous study, an important dimeric interfacial residue, Glu162, was replaced with aspartate and alanine. Glu162 interacts through a hydrogen bond with Glu162 and His163 of the adjacent subunit (Fig 1-1). The goals of this study were twofold: determine the role of Glu162 in structure and catalysis and compare the human E162A to the equivalent mutation in *E. coli* (Whittaker and Whittaker, 1998). The Glu170A mutant in *E. coli* is less stable, catalytically inactive and exhibits an altered metal specificity. Replacement of Glu162 in the human enzyme resulted in diminished catalysis and a higher degree of product inhibition than wild-type enzyme. A crystal structure of both E162A and E162D indicated an abolished interaction between the side chains of residues 162 and 163 though an intervening solvent molecule

bridged the interaction between Asp162 and His163 in the E162D mutant. Both mutants were tetrameric in solution and metal specificity was not altered for either mutant.

Structure of Nitrated Human MnSOD

The third goal was to establish a structural explanation for the decrease in catalysis observed when human MnSOD is nitrated at position 34. Previous studies have shown that nitration of Tyr34 in human MnSOD is associated with abolished catalysis, and recently this lab published the structure of nitrated MnSOD (Quint and Reutzel et al., 2005). Chapter 4 describes the first structure of a nitrated MnSOD. A 2.4 Å crystal structure of nitrated human MnSOD indicates exclusive nitration of Tyr34 though mass spectrometry indicates nitration of other positions. The orientation of the NO_2 group on 3-nitrotyrosine-34 suggests that steric blockade and potentially electronic repulsion of substrate could both cause catalytic inhibition.

CHAPTER 2
STRUCTURAL MOBILITY IN HUMAN MANGANESE SUPEROXIDE DISMUTASE

Introduction

The presence of a tetrameric interface in human MnSOD suggests enhanced stability; the *E. coli* dimeric MnSOD has a melting temperature of 76^{o}C compared to 90^{o}C for human, tetrameric MnSOD. A polymorphism in the tetrameric interface of human MnSOD, I58T, is associated with 50% decreased activity compared to wild type MnSOD and its melting temperature is decreased to 76^{o} C (Borgstahl et al., 1996). In addition, the heat extremophile *Thermus thermophilus* utilizes a tetrameric MnSOD (Wagner et al., 1993). This also suggests a role for the tetrameric interface in thermal stability.

The properties of the dimeric and tetrameric interfaces in human MnSOD have been investigated using ^{19}F NMR. Human MnSOD has been prepared with all nine tyrosine residues of each subunit replaced by 3-fluorotyrosine (abbreviated Fluoro-MnSOD) (Fig 2-1). The use of ^{19}F labels allows the observation of specific, well-resolved NMR signals of labeled-tyrosine residues at the dimeric and tetrameric interfaces. The NMR frequency of ^{19}F resonances are nearly as high as ^{1}H, thus producing about the same signal-to-noise as ^{1}H. Moreover, they have a much larger chemical shift range than ^{1}H, making them considerably more sensitive to local electronic environment. The replacement of hydrogen by fluorine in 3-fluorotyrosine is a minor steric change since the van der Waals radius of a fluorine is just 0.15 Å larger than the hydrogen it replaces

(Bondi, 1993), and the C-F moiety is a rather weak hydrogen bond acceptor (Jeffrey, 1997).

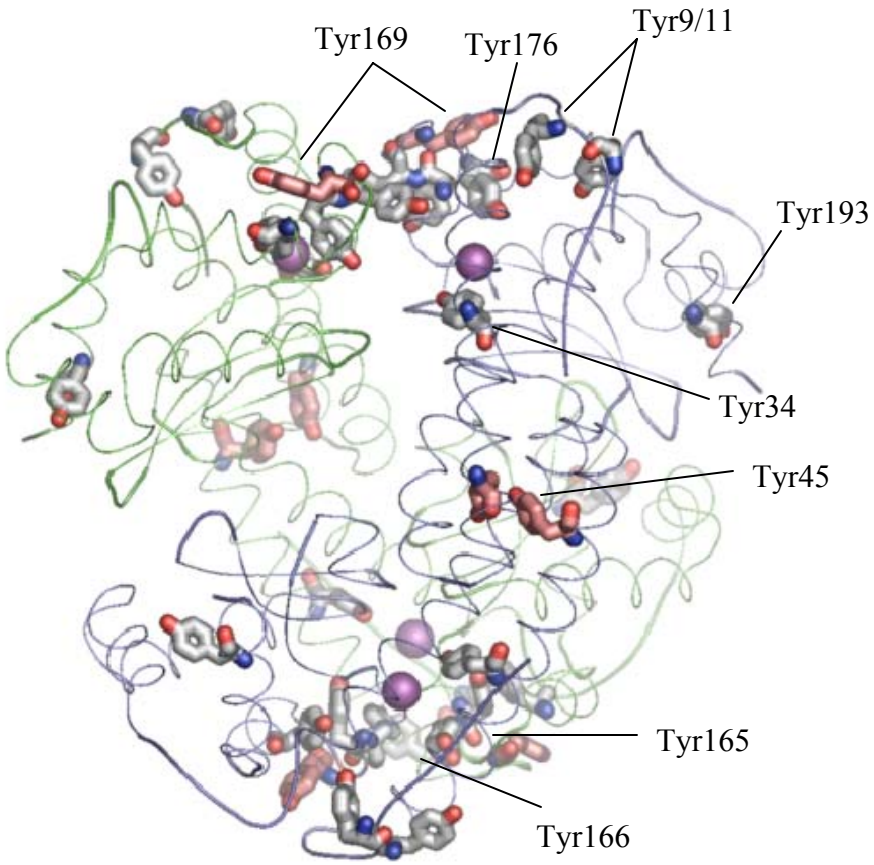

Figure 2-1 Structure of human MnSOD showing the dimeric and tetrameric interfaces. Also shown are the positions of five tyrosine residues that give sharp ^{19}F resonances when labeled with fluorine. Tyr45 is located at the tetrameric and Tyr169 at the dimeric interfaces.

The replacement of all tyrosines with 3-fluorotyrosine in human MnSOD has no observed effect on the structure of the enzyme as determined by X-ray crystallography at 1.5 Å resolution (Ayala et al., 2005); the fluorinated and unfluorinated structures are closely superimposable with the root-mean-square deviation for 198 α-carbon atoms at 0.3 Å (Ayala et al., 2005). We point out that the crystal structure of Fluoro-MnSOD showed a single side chain rotamer for each of the nine 3-fluorotyrosines (Ayala et al.,

2005). The catalytic activity of Fluoro-MnSOD was lower than that of MnSOD by a factor of 25 (Ren et al., 2005). This decrease could not be attributed to a single 3-fluorotyrosine residue, and was not primarily due to 3-fluorotyrosine at residue 34, which is in the active site.

The ^{19}F NMR show that Tyr169 at the dimeric interface of human MnSOD (Figure 2-1), has significantly less conformational freedom or mobility than does Tyr45 at the tetrameric interface. Consistent with these results, differential scanning calorimetry of human MnSOD showed that replacement by site-specific mutagenesis of Tyr169 at the dimeric interface decreased thermal stability and replacement of Tyr45 at the tetrameric interface did not. These results are discussed in terms of catalysis and stability of MnSOD.

Materials and Methods

Labeling with Fluorotyrosine, Expression in E. coli, and Purification

E. coli that express wild-type and the site-directed mutants of human MnSOD were grown for 17 hours at 37°C in 50 mL of minimal media. The minimal medium (M9), which consisted of 0.06 M phosphate buffer at pH 8.2, 8.6 mM NaCl, and 0.02 M NH_4Cl, was sterilized by autoclaving. The overnight culture was supplemented with 0.1 mM $CaCl_2$, 1 mM $MgSO_4$, 11 mM glucose, 1 μg/mL of thiamine, 0.2 mg/mL of amino acids (except the aromatic amino acids), 1 mM tryptophan, 1 mM phenylalanine, and ampicillin. The overnight growth was then transferred to 7.5 L of minimal media and supplemented in the same manner as the overnight culture plus the addition of $MnSO_4$ to 18 μM. The cells were allowed to grow for approximately 5 hours until an OD_{595} of 0.3-0.4 was reached. At this point, the cells were induced with 0.3 mM IPTG and supplemented with 1 mM 3-fluorotyrosine (or unlabeled L-tyrosine as a control) and were

allowed to grow for an additional 4 hours. Due to the low solubility of L-tyrosine and its fluorinated analog in water, these compounds were added as solids to the growing media. The cells were placed at 4°C overnight and harvested the next day by centrifugation. The resulting pellet was frozen at -70°C overnight and the pellet was then lysed the following day.

Depending on the particular sample preparation, the amount of 3-fluorotyrosine incorporated into MnSOD was 67% to 76%, as determined by amino acid analysis composition (Protein Chemistry Laboratory, Texas A&M University, College Station, TX) and corroborated by hybrid LCQ-ToF (QSTAR) mass spectrometry (ICBR, University of Florida, Gainesville, FL).

Site-Directed Mutagenesis of Fluorine Manganese Superoxide Dismutase

Site-directed mutants of human Fluoro-MnSOD were constructed for the purpose of assigning ^{19}F spectra of enzyme containing 3-fluorotyrosine. Each tyrosine of the enzyme was replaced individually by phenylalanine. An exception was the double mutant Y9F-Y11F; since these residues are near in sequence and tertiary structure we replaced these together. These mutants were generated with the Stratagene® QuikChange® Site-Directed Mutagenesis Kit (La Jolla, CA) in a Perkin Elmer GeneAmp PCR System 2400 (Foster City, CA). The plasmid of wild type MnSOD contained in the pTrc99A vector was used as the template. PCR was performed using specific oligonucleotides (Sigma-Genosys, The Woodlands, TX) containing the desired mutations as primers. The PCR products were digested with the restriction enzyme *Dpn I* and transformed into supercompetent XL-1 cells for selection. The plasmid containing the mutation of interest was isolated using the plasmid mini prep kit from Qiagen® and the mutation was corroborated by DNA sequencing of the entire coding region (ICBR, University of

Florida, Gainesville, FL). The plasmid containing the desired mutation was then transformed into QC774 cells from *E. coli*. This particular strain lacks the genes that encode for endogenous FeSOD (*SodB*$^-$) and MnSOD (*SodA*$^-$).

Amide Hydrogen/Deuterium Exchange Kinetics.

We employed amide H/D exchange mass spectrometry to examine backbone dynamics for human MnSOD (not fluorinated). By measuring the rate of amide H/D exchange over defined regions of human MnSOD, we were able to develop a comprehensive map of backbone dynamics that was complementary to the NMR studies. On-exchange experiments of amide backbone hydrogens with deuterium were performed in triplicate and involved exposing native human MnSOD to solvent 80% D_2O for 0, 1, 15, 300, 900, 1800, 3600, and 12000 s prior to quenching of amide hydrogen exchange by rapidly lowering the solution pH and temperature. After quenching, the protein was digested by exposure to pepsin, and the resultant peptide pool was examined by LC-MS. The uptake of deuterium for MnSOD pepsin-derived peptides was determined by measuring the increase in number-average *m*/*z* values of the ion isotopic distributions for each peptide from an on-exchange time point (deuterated peptide) when compared to the same peptide from $t = 0$ (nondeuterated peptide). The percent deuterium incorporation was determined for each peptide by dividing the measured number of deuterium atoms incorporated by the calculated number of exchangeable amide hydrogen atoms for that peptide

19F Nuclear Magnetic Resonance Spectroscopy

The ^{19}F NMR spectra of fluorinated samples were recorded on a Bruker Avance 500 MHz spectrometer. A ^{1}H 5mm TXI probe tuned for ^{19}F at 470 MHz was employed. We were not able to use a fluorine specific probe; the probe used displayed a very broad

background ^{19}F resonance upon which the peaks of our enzyme were superimposed. This arrangement precluded measurements of T_2 and we report linewidths instead. Due to this broad fluorine background, a T_2 filter was utilized. This allows for the broader signals of the spectrum to decay before the start of the data collection. The enzyme concentrations were 0.5 mM in phosphate buffer at pH 7.8, unless otherwise specified, and 10% (by volume) D_2O for an internal lock. Chemical shifts were referenced to the internal standard trifluoroacetate (TFA) at 0 ppm; high-field or shielded values with respect to TFA are taken as negative. Temperature was varied from 17^o C to 62^o C by the flow of heated nitrogen gas. Spectra were acquired by averaging 4000 scans with a scan rate of 8000 per hour.

Differential Scanning Calorimetry

Proteins were prepared in potassium phosphate buffer (20 mM, pH 7.8) at a concentration of 1 mg/ml. A solution of 20 mM potassium phosphate (pH 7.8) was used as a buffer reference. Both the sample and reference were degassed for 10 minutes before scanning from 25^0C to 120^0C at a rate of 1^0C per minute (Microcal VP-DSC). A buffer blank was subtracted from the final protein scan and a cubic baseline was fit to the profile. Changes in heat capacity (ΔC_p) for the unfolding peaks were corrected by fitting a non-two state model with a single component. Baseline correction and peak fitting were performed using Origin (Microcal Software, Northampton, MA).

Results

Assignment of Fluorine Resonances

There are nine 3-fluorotyrosine residues in each subunit of the tetramer in human wild-type Fluoro-MnSOD; five appear as distinct major peaks spanning about 8 ppm in the ^{19}F NMR spectrum (Figure 2-2). The integrated intensity of each individual peak was

approximately the same and represents one fluorine atom each. The assignment of the peaks in Figure 2 was achieved by measuring the ^{19}F NMR spectra of individual site-specific mutants in which each tyrosine was replaced by phenylalanine (Figure 2-2). Since residues 9 and ll are near each other in sequence, we saved effort by preparing the double mutant; hence, the NMR resonance assignments are not yet verified. However, in the crystal structure of Fluoro-MnSOD (Ayala et al., 2005; PDB # 1XDC) the side chain of Fluor-Tyr9 is buried with the phenolic hydroxyl hydrogen bonded to the backbone carbonyl of residue 78 and in near van der Waals contact with Pro8, suggesting the downfield shifted ^{19}F resonance of residue 9 with respect to Fluoro-Tyr11. Tyr11 is more exposed to the solvent than Tyr9. Thus we assign the more downfield resonance at -57.6 ppm to Tyr9 and the resonance at -60.1 ppm to Tyr11 (Figure 2-3). For reference, the ^{19}F resonance for monomeric tyrosine (pH 7.8, 25 ^{o}C) is -61.4 ppm, and the chemical shift of the single large resonance of collapsed Fluoro-MnSOD collapses at 62^{o} C is -62.3 ppm.

Of the nine 3-fluorotyrosine residues of each monomer, four are not observed in the ^{19}F NMR spectrum under the conditions of Figure 2-2. These are residues 34, 165, 166, and 176, the side chains of which are located at distances less than 9 Å from the manganese (manganese to hydroxyl distance). All of the observed resonances, residues 9, 11, 45, 169, and 193, are located at distances greater than 13 Å from the manganese. Thus it is a reasonable suggestion that the four residues of 3-fluorotyrosine not observed are broadened by the paramagnetic manganese, in addition to broadening by the overall slow motion of the homotetramer. At the pH 7.8 of these studies it is not expected that any of the tyrosine residues are ionized, consistent with literature on structure (Borgstahl et al., 1996) and catalysis (Hsu et al., 1996).

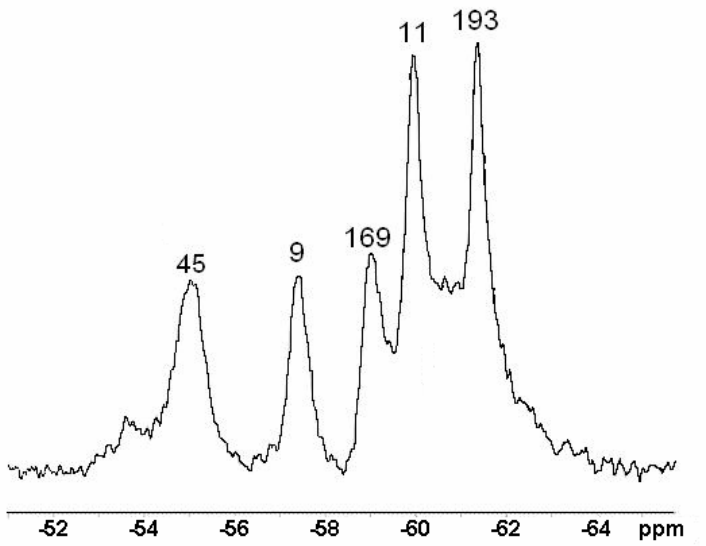

Figure 2-2 ^{19}F NMR spectrum (470 MHz) of wild-type human MnSOD in which all nine tyrosines were replaced with 3-fluorotyrosine. Residue assignments were made by replacement of individual 3-fluorotyrosine residues with Phe and are written above the peaks. Chemical shifts referenced to TFA as internal standard.

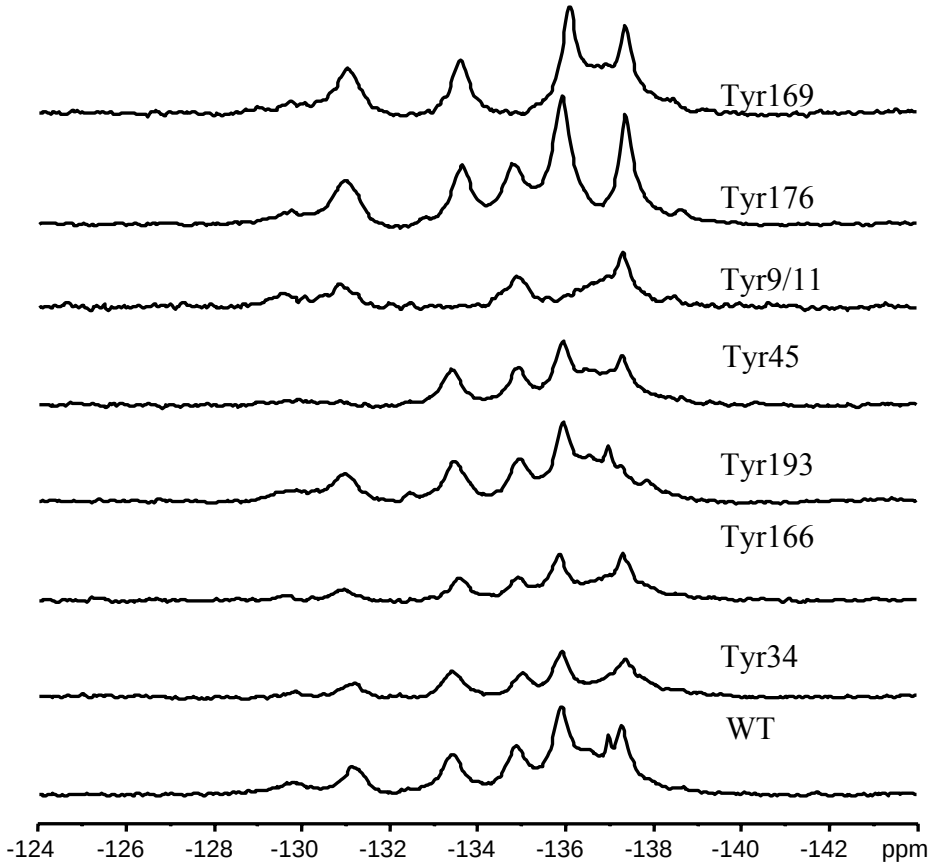

Figure 2-3 Stacked fluorine NMR spectra for wild-type human MnSOD in which tyrosines 9, 11, 34, 45, 166, 176 and 193 have been mutated to phenlylalanine.

Thermal Stability

Differential scanning calorimetry was used to determine changes in thermal stability for two unfluorinated mutants of human MnSOD at positions 45 and 169 measuring the main unfolding transition of the enzyme. The mutant with Tyr45 replaced by Ala exhibited an unfolding temperature of 94.3^{o} C compared to 90.7^{o} C for the wild type MnSOD (Hsu et al., 1996; Greenleaf et al., 2004)(standard deviation estimated at 0.3 ^{o}C). The unfolding temperature for the mutant with Tyr169 replaced with Ala was decreased to 86.5^{o} C. These site-specific mutants, one with Tyr45 replaced by Ala and the second with Tyr169 also replaced by Ala, showed no significant change in catalytic decay of superoxide measured by pulse radiolysis at Brookhaven National Lab (data not shown). Analysis by native polyacrylamide gel electrophoresis indicated that both mutants, Y45A and Y169A, remained tetrameric in solution.

Temperature Dependence of Fluorine Resonances

The change as temperature was increased from 17^{o} to 57^{o} C in the chemical shifts of each of the five assigned resonances was uniform with no significant changes in slope for individual peaks over this temperature range (Figure 2-3). The two residues that had the largest downfield ^{19}F chemical shift, Fluoro-Tyr45 and Fluoro-Tyr9, also showed the largest changes in chemical shift (Figure 2-3) and in linewidth at half height (Figure 2-4) as temperature increased. The remaining assigned residues Fluoro-Tyr11, 169, and 193 showed smaller changes in chemical shifts and in linewidths with changes in temperature over the range of temperatures in Figures 2-4 and 2-5. It is notable that Fluoro-Tyr169, iun the dimeric interface, showed almost no change in linewidth with temperature (Figure 2-5).

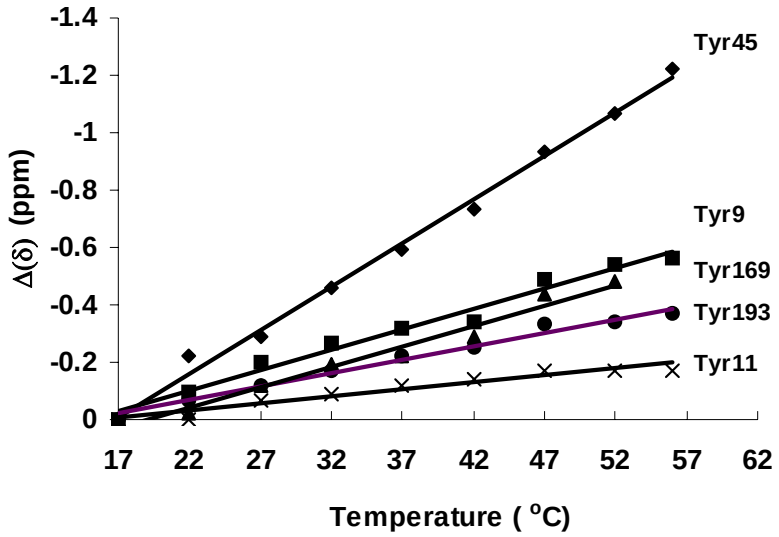

Figure 2-4 The temperature dependence of five 19F chemical shifts of wild-type human MnSOD in which all tyrosine residues are replaced with 3-fluorotyrosine. Values are normalized to show a single chemical shift at 17o C in order to compare trends. Conditions are as described in Figure 2-2. (◆) Tyr45; (■) Tyr9; (▲)Tyr169; (●) Tyr193; (✕)Tyr11.

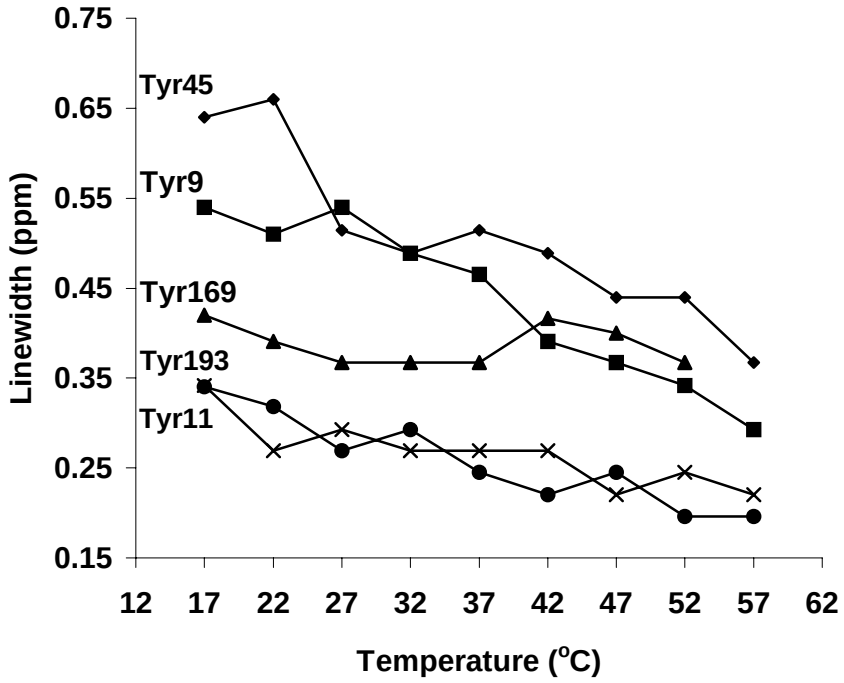

Figure 2-5 The temperature dependence of ^{19}F linewidths at half height for wild-type human MnSOD in which all tyrosine residues are replaced with 3-fluorotyrosine. Conditions are as described in Figure 2-2. (◆) Tyr45; (■) Tyr9; (▲)Tyr169; (●) Tyr193; (✕)Tyr11.

To corroborate these findings, hydrogen/deuterium exchange studies were performed. Using this approach, amide hydrogen exchange kinetics of 29 peptides (comprising approximately 78% of the human MnSOD protein) were determined (Figure 2-6). For each peptide, the percentage of deuterium uptake versus time for the seven on-exchange time intervals was plotted with error bars (plots not shown) representing the mean standard deviation of the deuterium incorporation percentages determined from triplicate experiments. The rate of deuterium incorporation varied in different regions of the protein (Figure 2-6). Peptides corresponding to regions 25-40, 58-77, and 94-113 displayed significant protection from amide H/D exchange as demonstrated by very low levels of deuterium incorporation with their maximum levels being below 35% (percent of the maximum on-exchange possible corrected for percent deuterium exposure and back exchange) at the longest on-exchange time point. Peptides corresponding to regions 1-20, 78-96, 114-135, and 155-173 showed moderate protection from amide H/D exchange with levels of deuterium incorporation between 50% and 60% at the longest on-exchange time point.

Discussion

Emphasized here are the properties of Fluoro-Tyr45 and 169, which are located in the tetrameric and dimeric interfaces, respectively (Figure 2-1). The ^{19}F resonance of Fluoro-Tyr45 showed a large increase in chemical shift as temperature increased (Figure 2-4), moving toward the position of the ^{19}F peak for denatured enzyme, and showed a large decrease in linewidth as temperature increased (Figure 2-5). These features characterize a region at the tetrameric interface with increased conformational and dynamic mobility as temperature increases. Based on previous studies of the motions of

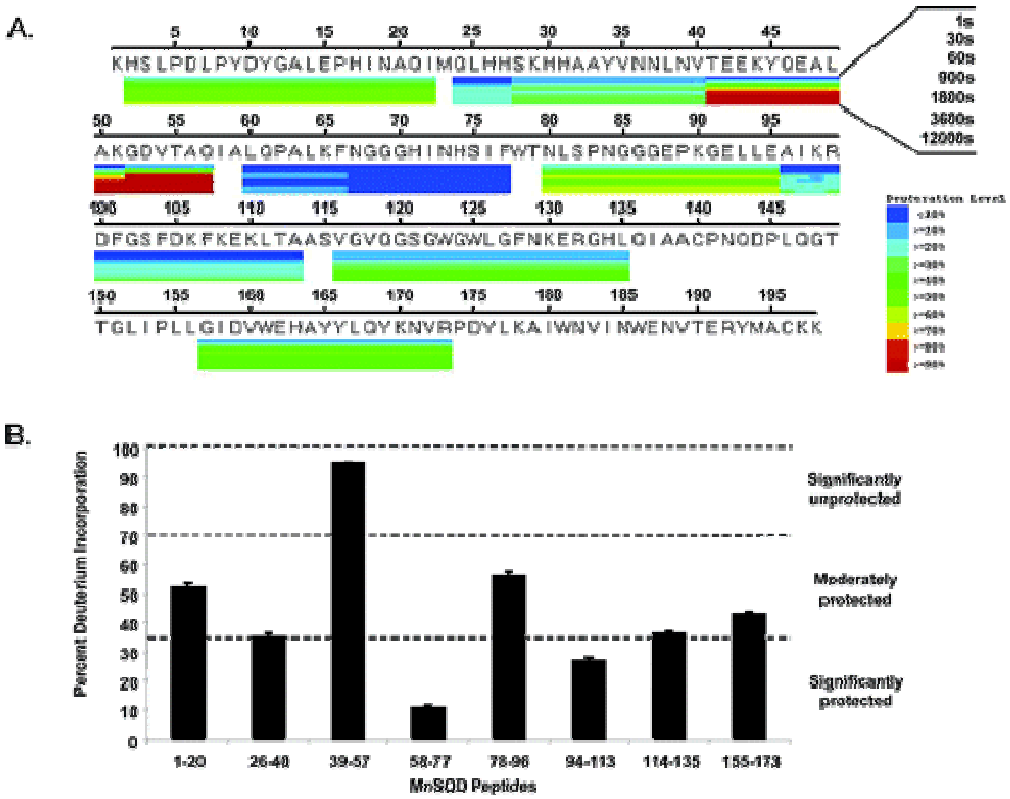

Figure 2-6 H/D exchange map for human MnSOD. Each block represents a pepsin-derived fragment of MnSOD detected by LC-MS and monitored during on-exchange time periods to determine the degree of deuterium incorporation. The gradations within each block represent the seven on-exchange time periods used with the shortest period being on top. The deuteration level, as a percentage of the theoretical maximum, for each peptide at each time period is color-coded.

fluorotyrosine rings in proteins (Hull and Sykes, 1975; Hull and Sykes, 1975B), we anticipate that the dominant spin-lattice relaxation mechanism is dipolar with a contribution from chemical shift anisotropy, and that the decrease in linewidths observed in ^{19}F resonances can be largely attributed to motional narrowing. We point out that the crystal structure shows just one rotamer for the side-chains of each 3-fluorotyrosine residue in Fluoro-MnSOD (Ayala et al., 2005); although we cannot exclude a contribution of chemical exchange to line broadening, neither the crystal structure nor the observed ^{19}F spectrum suggest that such a mechanism is predominant.

The ^{19}F resonance of Fluoro-Tyr169 is notable because it does not change appreciably in linewidth over the temperature range from 17^{o} to 57 ^{o}C (Figure 2-5). The other ^{19}F resonances have linewidths that decrease with increasing temperature, suggesting increasing motional processes; Fluoro-Tyr169 does not show a detectably higher degree of motional freedom as temperature increases. Also, Fluoro-Tyr169 shows a chemical shift change as temperature increases that is modest compared with that of Fluoro-Tyr45 (Figure 2-4). The linewidth data especially indicate that the environment of this side chain is rather stable with little change in mobility over the temperature range studied. Residue 169 is located at the dimeric interface and its side chain appears in near van der Waals contact with the hydrocarbon side chain of Gln168. Considering residue 169 as a reporter for the dimeric interface, these data indicate stability and lower motional freedom for the region of Fluoro-Tyr169.

Of the remaining observed ^{19}F resonances, those of residues 11 and 193 had chemical shifts closest to monomeric 3-fluorotyrosine or to partially denatured Fluoro-MnSOD. With increasing temperature, their chemical shifts moved toward that of the denatured enzyme and their linewidths narrowed somewhat (Figures 2-4, 2-5). These features are consistent with the partially constrained positions of Tyr11 and 193 in the structure. Fluoro-Tyr9 was different in showing a rather substantial temperature effect in its ^{19}F linewidth (Figure 2-5), although showing a rather modest temperature effect on ^{19}F chemical shift (Figure 2-4).

Deutrium exchange studies on native MnSOD corroborate the findings of fluorine NMR. The most rapidly exchanging MnSOD peptides, or regions of MnSOD that demonstrate little or no protection to amide H/D exchange, were in the 40-58 region that

showed 96% deuterium incorporation at the 3600 s time point. The exchange kinetics for a region of a protein is dependent in part on the extent of localized hydrogen bonding as amide hydrogens are protected from exchange while involved in hydrogen bonding. For an amide hydrogen involved in a hydrogen bond to become exchange competent, localized unfolding must occur to break the hydrogen bond and allow exchange with solvent protons or deuterons. Therefore, slowly exchanging regions of a protein are considered less dynamic in part due to significant hydrogen bonding. Taken together, the data indicate that the regions corresponding to the tetrameric domain (40-58) and the dimeric domain (159-174) display different amide H/D exchange kinetics with the tetrameric domain affording rapid exchange and the dimeric domain affording moderate protection from amide H/D exchange (Figure 2-6)

The thermal unfolding data appear consistent with these conclusions. Specifically, differential scanning calorimetry showed that replacement of Tyr169 with Ala destabilized human MnSOD with the major unfolding transition decreased about 4^{o} C compared with wild type, while the replacement of Tyr45 did not destabilize but actually enhanced stability somewhat. The observation that the melting temperature for Y169A is decreased unlike the Y45A mutant suggests that the dimeric interface is stabilized by specific residue interactions whereas the tetrameric interface is stabilized by several non-specific interactions.

Evolution clearly shows a dimeric MnSOD of primitive species, with tetrameric MnSOD a different development (Purrelo et al., 2005). In fact, crossing the dimeric interface are residues such as Glu162 and Tyr166 that extend into the active site of the adjacent subunit and are significant contributors to catalysis (Whittaker and Whittaker,

1998; Hearn et al., 2004). In human MnSOD, the reporter residue at the dimeric interface Tyr169 showed less conformational mobility and greater contribution to stability than Tyr45 at the tetrameric interface. This may in part reflect the observation that residues at the dimeric interface are closer to the active site, likely play a greater role in supporting catalysis, and hence require a greater degree of conformational stiffness than residues at the tetrameric interface.

CHAPTER 3
ROLE OF A GLUTAMATE BRIDGE SPANNING THE DIMERIC INTERFACE OF HUMAN MANGANESE SUPEROXIDE DISMUTASE

Introduction

The previous chapter elucidated the roles of the tetrameric and dimeric interfaces and their contribution to enzyme stability. Recognizing the role of the dimeric interface in catalysis, this chapter focuses on a mutation in the dimeric interface and the subsequent effects on catalysis and stability. This study reports the role of Glu162 in human MnSOD, the side chain carboxyl of which forms a hydrogen bond with the imidazole side chain of His163 of the adjacent subunit, a ligand of the metal (Figure 3-1). Using both X-ray crystallography and pulse radiolysis, reported here are the effects of mutation of Glu162 to aspartate and alanine. The X-ray data for E162D and E162A reveal no significant structural changes compared with wild type other than the lost interaction with His163, and in the case of E162D an intervening water molecule maintains a hydrogen-bond link between Asp162 and His163. However, mutation of Glu162 introduces a pH dependence in catalysis and in the visible absorption spectrum of Mn^{3+}SOD near pK_a 8.5 not observed in human wild-type MnSOD. Mutation of Glu162 to either aspartate or alanine results in a greater degree of product inhibition compared to wild-type MnSOD. Differential scanning calorimetry indicates that the hydrogen bond between Glu162 and His163 contributes to the stability of MnSOD. These data emphasize the role of the dimeric interface of human MnSOD in catalysis and thermal stability.

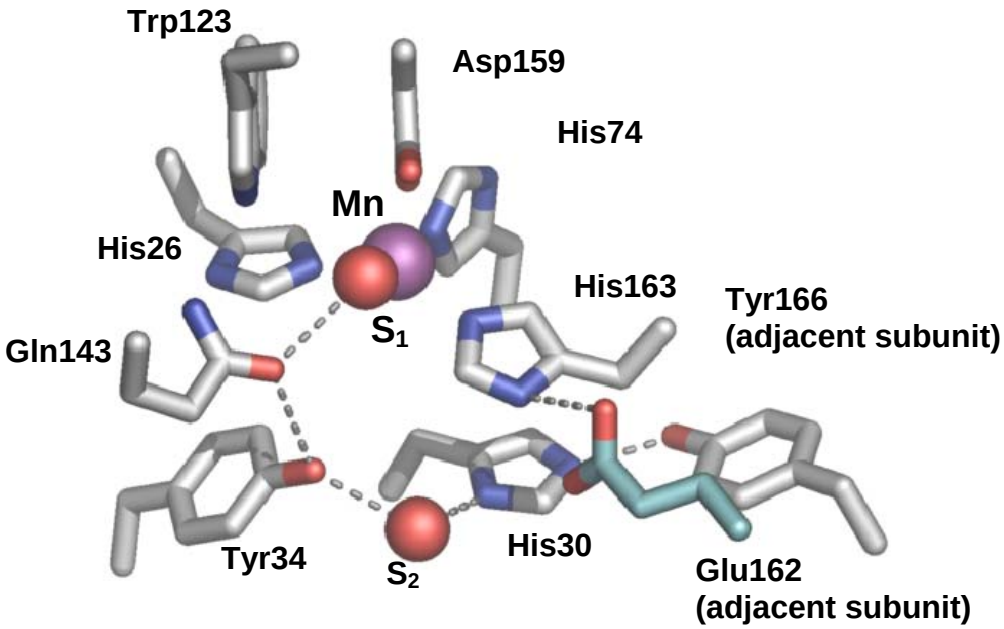

Figure 3-1 Active-site structure including the hydrogen bond network for human wild-type MnSOD (Borgstahl et al., 1992). The manganese is designated as a purple sphere and solvent molecules as red spheres. Dotted lines indicate a hydrogen-bonded network emanating from the metal-bound solvent molecule to Tyr166 from an adjacent subunit.

Materials and Methods

Site Directed Mutagenesis

Mutants were generated with the Stratagene® QuikChange® Site-Directed Mutagenesis Kit (La Jolla, CA) in a Perkin Elmer GeneAmp PCR System 2400 (Foster City, CA). The plasmid of wild type MnSOD contained in the pTrc99A vector was used as the template. PCR was performed using specific oligonucleotides (Sigma-Genosys, The Woodlands, TX) containing the desired mutations as primers. The PCR products were digested with the restriction enzyme *Dpn I* and transformed into supercompetent XL-1 cells for selection. The plasmid containing the mutation of interest was isolated using the plasmid mini prep kit from Qiagen® and the mutation was corroborated by DNA sequencing of the entire coding region (ICBR, University of Florida, Gainesville,

FL). The plasmid containing the desired mutation was then transformed into QC774 cells from *E. coli*. This particular strain lacks the genes that encode for endogenous FeSOD (*SodB*$^-$) and MnSOD (*SodA*$^-$).

Expression and Purification of Human MnSOD

The pTrc99A plasmid containing the mutant MnSOD template was transformed into *SodA*$^-$/*SodB*$^-$ *E. coli* QC774 cells. Cells were grown in luria broth media supplemented with 6 mM $MnCl_2$ and ampicillin for selection. Cultures were grown to 0.8 absorbance units and then induced with IPTG. Cells were centrifuged and then lysed. The lysate was heat treated at 60^o C for 15 minutes to select for MnSOD, which is thermostable to 70^o C. Following heat treatment, the lysate was spun and the supernatant was dialysed against three exchanges of 20 mM Tris pH 8.2 and 50 μM EDTA. The dialysate was purified using a Q-sepharose anion exchange column (Pharmacia). Protein concentrations were determined by UV spectrometry using a Beckman Coulter DU 800 spectrometer at 25^o C and pH 7.8 (ε_{280} = 40,500 M^{-1} cm^{-1}) (Greenleaf et al., 2004). Manganese and iron content for each enzyme sample were determined using flame atomic absorption spectroscopy (flame AA), and division by the total protein concentration gives metal occupancy for the enzyme.

Visible Absorption

The visible spectrum for human MnSOD shows a broad absorption with a maximum at 480 nm (ε_{480} = 610 M^{-1} cm^{-1}) (Hsu et al., 1996). Profiles for pH dependence were determined by measuring the absorption at 482 nm at pH varying from 6.5 to 11.5. Enzyme samples were diluted 1:1 (~500 μM enzyme) in a buffer containing 200 mM

MES and 200 mM TAPS and pH was adjusted using 5 M KOH. The pH was measured using a Fisher Accumet 610 pH meter with a Corning semi-micro combo electrode.

Pulse Radiolysis

Pulse radiolysis experiments were performed at Brookhaven National Lab using a 2 MeV van de Graff generator to produce superoxide directly in solution. Superoxide radicals were formed by exposing aqueous, air-saturated solutions to a high-dose electron pulse according to methods described by Schwarz (Schwarz, 1981). Up to 45 μM superoxide was produced in solution. Enzyme solutions contained 2 mM buffer containing either MOPS pH 6.5-8.0, TAPS 8.0-9.0, or CAPS 9.0-10.0 depending on the desired pH, 50 μM EDTA, and 30 mM formate to scavenge hydroxyl radicals. The reactions were monitored spectrophotometrically using a Cary 210 spectrophotometer at 25^{o} C by following changes in the absorbance of superoxide (ε_{260} = 2000 M^{-1} cm^{-1}) (Rabini and Nielson, 1969) or by following enzyme absorbance at 420 nm or 480 nm (Cabelli et al., 1999).

Manganese and Iron Content Determination

Flame atomic absorption spectroscopy was used to determine total metal content in all enzyme solutions. A Perkin Elemer 308 Flame Atomic Absorption Spectrometer was utilized to determine manganese concentration. A multi-ion lamp with a 3-slit burner was used and absorption was measured at 279 nm. Manganese occupancies were determined by dividing the total metal concentration by the enzyme concentration to yield a percentage of total active sites containing manganese. Typical occupancies for metal in the active site range from 70% to 90%. Iron content was measured by ABC Research Corp (Gainesville, FL) and was determined to account for less than 2% of the total metal

in solution E162D and E162A MnSOD. The manganese concentration was used as the active enzyme concentration for all pulse radiolysis measurements.

Crystallography

Hexagonal crystals were grown from a solution of 3 M ammonium sulfate containing 100 mM imidazole and 100 mM malate at pH 7.8-8.2 using the vapor diffusion method. Crystals approximately 0.2 x 0.2 x 0.3 mm grew within one week and were magenta in color. Diffraction data were collected from single crystals wet mounted in quartz capillaries (Hampton Research) on an R-AXIS IV++ image plate (IP) system with Osmic mirrors and a Rigaku HU-H3R CU rotating anode operating at 50 kV and 100 mA (Rigaku/MSC). Diffraction data was collected at room temperature. A 0.3 mm collimator was used with a crystal to IP distance of 220 mm and the 2θ angle fixed at 0^{o}. The frames were collected using a 0.3^{o} oscillation angle with an exposure time of 5 min/frame at room temperature. Both data sets were indexed using DENZO and scaled and reduced with SCALEPACK software (Otwinowski, 1997). Diffraction intensities were visible to 2.3 Å resolution for E162D and 2.5 Å for E162A. Diffraction and refinement statistics are given in Table 3-2.

To prevent model bias, human MnSOD mutants were phased using the human, wild-type MnSOD structure (Quint and Reutzel et al., 2006; PDB accession 2ADQ) from which the residue at position 162 was replaced with an alanine and the active-site manganese had been removed. The structures were phased and refined using the software package CNS (Brunger et al., 1998). Refinement cycling (using rigid body, simulated annealing for the first cycle, minimization, and individual B-factor refinement) was done

in conjunction with rounds of manual model building using the program COOT for molecular modeling (Emsley and Cowtan, 1998).

Differential Scanning Calorimetry

Enzyme samples were buffered in 20 mM potassium phosphate pH 7.8 at a concentration of 1 mg/ml. A solution of 20 mM potassium phosphate pH 7.8 was used as a buffer reference and was subtracted from the protein scan prior to baseline correction and model fitting. Both the sample and reference were degassed for 10 minutes before scanning from 25^{o} C to 110^{o} C at a rate of 1^{o} C per minute (Microcal VP-DSC). A buffer blank was subtracted from the final protein scan and a cubic baseline was fit to the profile. Changes in heat capacity (ΔC_p) for the thermal unfolding peaks were corrected by fitting a reversible, non-two state model with two components. Baseline correction and peak fitting were performed using the program Origin (Microcal Software, Northampton, MA).

Results

Visible Spectrometry

Atomic absorption spectroscopy for the mutants of MnSOD studied here showed that the metal occupancy for E162D was 88% Mn with <1% Fe, and the metal occupancy for E162A was 54% Mn and <1% Fe. Both mutants were tetramers as determined by non-denaturing PAGE. Human wild type Mn^{3+}SOD as well as E162D and E162A Mn^{3+}SOD exhibit a characteristic visible absorbance with a maximum at 480 nM (ε_{480} = 610 M^{-1} cm^{-1}) corresponding to Mn^{3+} in the active site (Hsu et al., 1996). The pH profile for molar absorptivity for wild-type human Mn^{3+}SOD fits a single ionization with a pK_a of 9.2 ± 0.1 (Figure 3-2) (Hsu et al., 1996; Greenleaf et al., 2004). Mutation to aspartate

resulted in a diminished pK_a ($pK_a = 8.7 \pm 0.2$) whereas replacement with alanine increased the pK_a ($pK_a = 10.1 \pm 0.1$) (Figure 3-2).

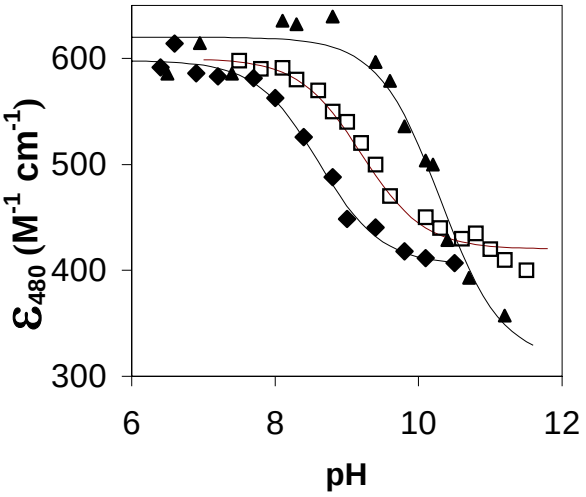

Figure 3-2 pH profile for molar absorptivity at 480 nm for (□) human wild-type Mn^{3+}SOD, (♦) E162D Mn^{3+}SOD and (▲) E162A Mn^{3+}SOD. Data were fit to a single ionization with values of pK_a 8.7 ± 0.2, 9.2 ± 0.1, and 10.1 ± 0.1 for E162D, wild type, and E162A Mn^{3+}SOD respectively. Solutions contained 200 mM MES and TAPS at 25° C and pH was adjusted using 5 M KOH.

Catalysis

MnSOD catalyzes the disproportionation of superoxide through a two-step process in which the active-site metal cycles between the Mn^{3+} and Mn^{2+} states concomitant with oxidation and reduction of superoxide (shown in eqs. 3-1 and 3-2) (Hearn et al. 2001; McAdam et al., 1977; Cabelli et al., 1999).

$$Mn^{3+}(OH)SOD + O_2^{\cdot-} + H^+ \xrightarrow{k1} Mn^{2+}(H_2O)SOD + O_2 \quad (3\text{-}1)$$

$$Mn^{2+}(H_2O)SOD + O_2^{\cdot-} + H^+ \xrightarrow{k2} Mn^{3+}(OH)SOD + H_2O_2 \quad (3\text{-}2)$$

$$Mn^{2+}(H_2O)SOD + O_2^{\cdot-} \xrightarrow{k3} Mn^{3+}(O_2^{2-})SOD \quad (3\text{-}3)$$

$$Mn^{3+}(O_2^{2-})SOD + H^+ + H_2O \xrightarrow{k4} Mn^{3+}(OH)SOD + H_2O_2 \quad (3\text{-}4)$$

The scheme shown here reflects the observation that the solvent ligand of Mn^{3+}(OH)SOD takes up a proton upon reduction of the metal as shown in equation 3-1. Equations 3-3 and 3-4 represent the formation and dissociation of a product inhibited complex characterized by zero-order catalysis (Hearn et al., 2001; McAdam et al., 1977).

Estimation of the rate constants for eqs 3-1 through 3-4 were carried out by measuring the rate of change of absorbance of $O_2^{\bullet -}$ and of enzyme species after the generation of $O_2^{\bullet -}$ by pulse radiolysis (Hearn et al., 2001; Cabelli et al., 1999). Decrease in absorption at 260 nm (ε_{260} = 2000) (Rabini and Nielson, 1969) corresponds to the disappearance of superoxide catalyzed by wild type, E162D, and E162A MnSOD, which is characterized by a first-order phase of catalysis that is relatively uninhibited followed by a zero-order, product inhibited phase (Hsu et el., 1996; Bull, Yoshida and Fee, 1991). When enzyme and superoxide are similar in concentration, the progress curve for superoxide decay is dominated by the reaction in eq 3-1, and a rate constant for k_1 can be determined from a first-order fit to the decay. Another method for determining k_1, described by Hearn et al., 1999 (Borgstahl et al., 1996), involves measuring changes in absorption at 480 nm under single turnover conditions when there is a molar excess of enzyme. Decrease in absorption at 480 nm results from the conversion of Mn^{3+}SOD to Mn^{2+}SOD shown in eq 3-1. This is a complementary method for determining k_1 and values for the two methods are in agreement. After addition of a molar equivalent of H_2O_2 to reduce the active-site manganese to Mn^{2+}, observation of the increase in absorption at 480 nm yields an estimate for k_2 at earlier time points and k_4 at the later part of the curve. The product-inhibited complex has a characteristic absorption at 420 nm (Bull, Yoshida and Fee, 1991) and measuring absorption increase at 420 nm after

reduction of the enzyme with H_2O_2 allows for an estimate of the rate constant k_3 (Hearn et al., 2001). Figure 3-3 shows typical data generated for the calculation of k_3.

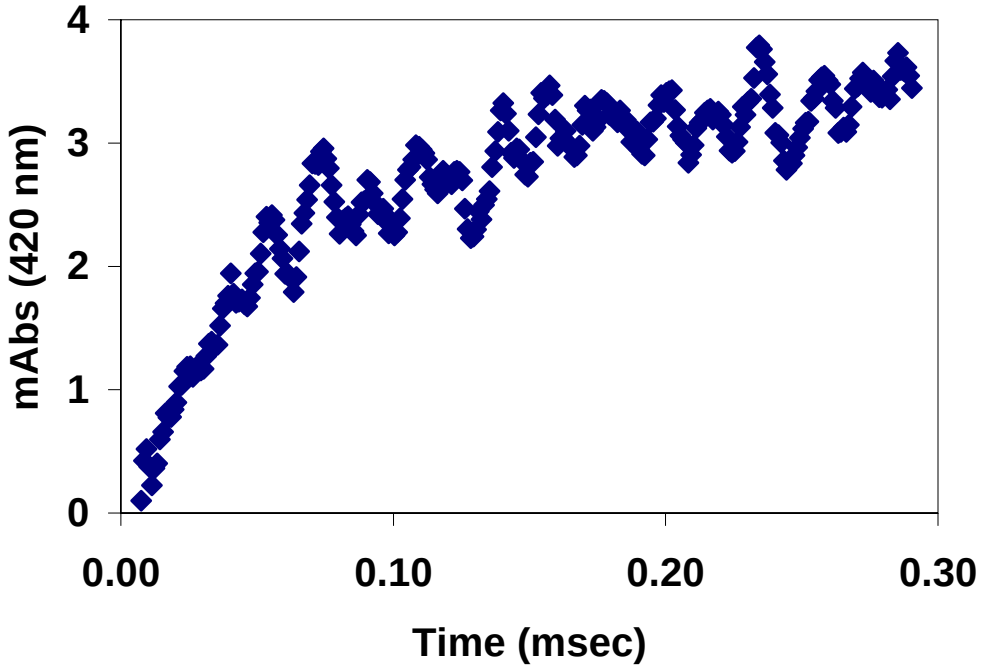

Figure 3-3 Change in absorbance at 420 nm over a millisecond timescale after generation of 5.6 μM superoxide by pulse radiolysis in a solution containing 120 μM E162D MnSOD buffered by 2 mM TAPS at pH 8.35 with 50 μM EDTA and 30 mM sodium formate at 25 ^{o}C. Prior to pulsing, the sample was reduced with 300 μM H_2O_2. Increase in absorbance at 420 nm was fit to a first-order process giving the rate constant 14.4 ms^{-1}.

The values of k_1-k_4 describing catalysis by human wild-type MnSOD are independent of pH in the range of pH 7 to 9.5 with a slight decrease above pH 9.5 (Greenleaf et al., 2004; Hearn et al., 2001). Values of the rate constants k_1-k_3 for catalysis by E162D MnSOD were pH dependent (Figure 3-4) and could be fit to a single ionization with maxima given in Table 3-1 and values of pK_a in the range of 8.0 to 8.7 given in the legend to Figure 3-4. The rate constant k_4 describing the dissociation of the product-inhibited complex was independent of pH though it was diminished three-fold compared

to wild-type enzyme. E162A MnSOD exhibited no pH dependence for k_1-k_3 with values given in Table 3-1 concomitant with oxidation and reduction of superoxide (shown in eqs. 3-1 and 3-2) (Hearn et al., 2001; Cabelli et al., 1999; McAdam et al., 1977). However, above pH 8.0, the rate constant k_4 was decreased 10-fold, from 30 ± 3 sec^{-1} to 3 ± 1 sec^{-1}.

Table 3-1 Maximal rate constants for the catalysis and inhibition of human wild type MnSOD and mutants.

	k_1 ($\mu M^{-1} sec^{-1}$)	k_2 ($\mu M^{-1} sec^{-1}$)	k_3 ($\mu M^{-1} sec^{-1}$)	k_4 (sec^{-1})
WT[b]	1500	1100	1100	120
E162D[a]	355 ± 33	133 ± 16	215 ± 20	40 ± 1
E162A[a]	63 ± 4	50 ± 4	87 ± 3	30 ± 3
H30N[c]	210	400	680	480
Y166F[d]	0.2	0.2	0.2	270
E. coli[e]	1000	800	150	60

(a) 2mM TAPS pH 7.7, 50mM EDTA, 30 mM formate (see methods for pulse radiolysis)
(b) Ramilo et al., 1998
(c) Hearn et al., 2003
(d) Hearn et al., 2001
(e) unpublished

The maximal value for the steady-state rate constant k_{cat}/K_m for E162D was 290 $\mu M^{-1} sec^{-1}$ compared to 800 $\mu M^{-1} sec^{-1}$ for wild-type enzyme, and decreased in a pH dependent manner with a pK_a of 8.8 (Figure 3-5). The maximal value for k_{cat}/K_m for E162A was diminished 8-fold (120 $\mu M^{-1} sec^{-1}$) independently of pH (Table 3-3). The rate constant k_0/[E] describes the product-inhibited, zero-order region of catalysis. The maximal value of k_0/[E] for E162D MnSOD was 270 sec^{-1} and was mostly pH independent, though there was a decrease at higher pH (190 sec^{-1} at pH 8.3) (Table 3-3). The E162A mutant exhibited a more extensive decrease with pH. The value for k_0/[E] at pH 7.7 was 190 sec^{-1} while at pH 8.4 it decreased to 18 sec^{-1}. For comparison, the value

of k_0/[E] is near 500 s^{-1} and is pH independent (Hearn et al., 2001; Hsu et al., 1996; Greenleaf et al., 2004) (Table 3-3).

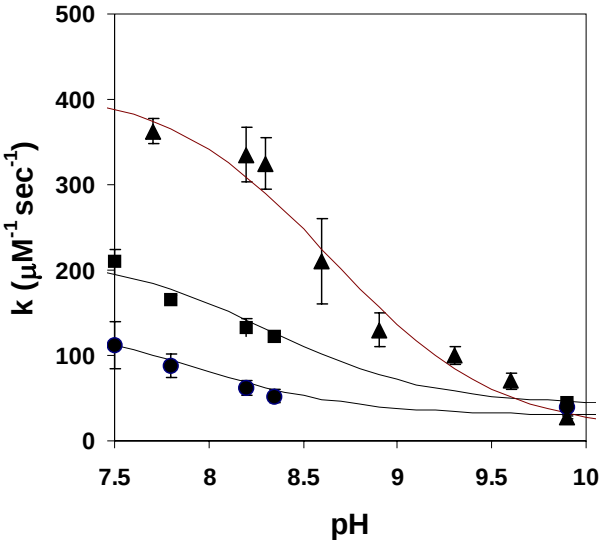

Figure 3-4 pH profile for k_1 (▲), k_2 (●), and (■) k_3 in catalysis of the disproportionation of superoxide by E162D MnSOD. Solutions contained 120 μM enzyme, 2 mM buffer (see methods), 50 μM EDTA and 30 mM sodium formate at 25° C. A single ionization was fit to the data with values for pK_a of 8.7 ± 0.2 for k_1 and 8.1 ± 0.1 and 8.0 ± 0.1 for k_2 and k_3 respectively.

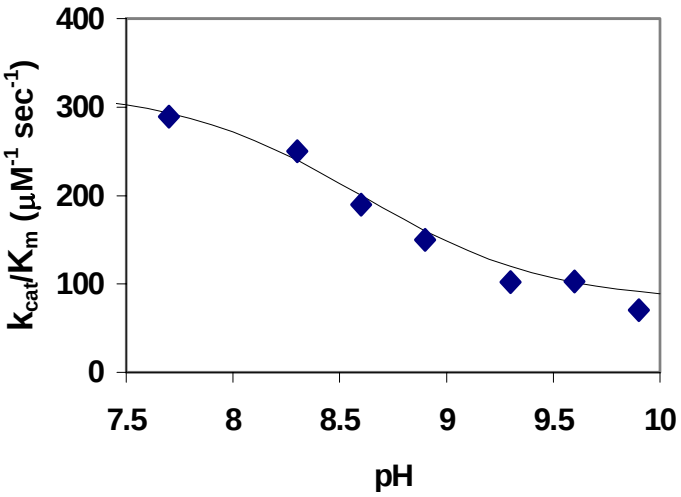

Figure 3-5 pH profile for K_{cat}/Km for E162D MnSOD. Solutions contained 2mM MOPS (pH 6.5-8.0), TAPS (8.0-9.0), or CAPS (9.0-10.0) 50 μM EDTA and 30 mM sodium formate at 25° C . The line represents a theoretical curve for a single ionization with value for pK_a of 8.8.

Structure of MnSOD Mutants

The human MnSOD mutants E162D and E162A crystallized in the hexagonal space group $P6_122$ under similar crystallization conditions (see methods) (Table 3-2). Both mutants contained a homodimer in the asymmetric unit with the eukaryotic tetramer formed from a crystallographic, symmetry-generated dimer. The models for the two mutants superimpose well on wild type (rmsd = .2 Å for E162D and .2 Å for E162A). The major difference is the truncation of the hydrogen bond interaction between Glu162 and His163 (Figures 3-6 and 3-7). The E162D structure retains an interaction with His163 through a solvent molecule (Figure 3-7). This interaction does not exist in the E612A mutant and therefore any stabilizing force that the residue at position 162 would have on His163 or the active site in general is missing. The positions of the active-site residues were altered for the two mutants. For E162A, the distances from Asp159 and His74 to manganese were decreased from 2.04 Å for wild type to 1.61 Å and from 2.23 Å to 1.65 Å respectively. Distances for the remaining coordinating residues were not significantly different. Distances were altered by < 10% for the E162D structure.

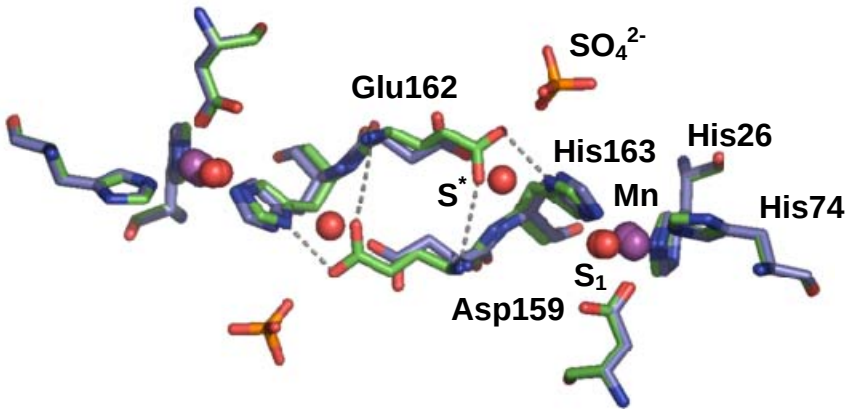

Figure 3-6 Structure of E162D MnSOD (shown in green) superimposed on wild-type human MnSOD (shown in blue) in the region of the mutated residue. Red spheres represent solvent and the manganese is shown in purple. The intervening solvent molecule from the E162D structure is labeled S*.

Table 3-2 Diffraction data and refinement statistics for human E162D and E162A MnSOD.

	E162D	**E162A**
Space group	$P6_122$	$P6_122$
Unit-cell parameters (Å)	a = 81.16, c = 241.17	a = 81.26, c = 242.28
	α = 90°, γ = 120°	α = 90°, γ = 120°
Resolution (Å)	20-2.3	20-2.5
No. of unique reflections	19557	16004
Completeness (%)	89.0 (90.3)	92.6 (93.8)
[a]R sym (%)	12.0 (21.0)	14.5 (46.0)
{I/σ (I)}	18.7 (19.7)	22.0 (7.2)
[b]R factor (%)	20.7	24.0
R free (%)	22.7	25.6
No. of protein atoms	1553	1550
No. of water molecules	51	38
[c]R.m.s.d. bond length (Å)	0.005	0.006
[c]R.m.s.d. bond angle (°)	1.199	1.426
Avg B (main/side/solvent)	25.2/28.1/34.7	32.6/34.1/34.6
Ramachandran Plot (%)		
Most favored regions	92.1	91.5
Addn'l allowed regions	6.7	7.3
Gen allowed regions	1.2	1.2
Disallowed regions	0	0

Data collected at room temperature
*Data for the highest resolution shell are given in parentheses.
[a]$R_{sym} = \Sigma |I-\langle I\rangle| / \Sigma I \times 100$, where I is the intensity of a reflection and <I> is the average intensity.
[b]$R_{factor} = \Sigma_{hkl} |F_o-KF_c| / \Sigma_{hkl} |F_o| \times 100$, R_{free} is calculated from 5% randomly selected data for cross-validation.
[c]R.m.s.d. = root mean square deviation.

Thermal Stability

Differential scanning calorimetry was used to determine thermal transition temperatures for E162D and E162A human MnSOD. E162D MnSOD showed two peaks and these melting temperatures were quite similar to those observed for wild type. The thermal inactivation temperature was 72° C and the unfolding temperature was 88° C.

These values for wild-type human MnSOD were 68° C and 90° C, respectively (Borgstahl et al., 1996). Replacement with alanine destabilized the enzyme. E162A MnSOD exhibited a split peak with values of 74.5° C and 81° C. The calorimetric data for both mutants were the composite of three experiments averaged and normalized to a non-two state model with two components. Melting temperatures for E162D and E162A were determined at pH 7.8.

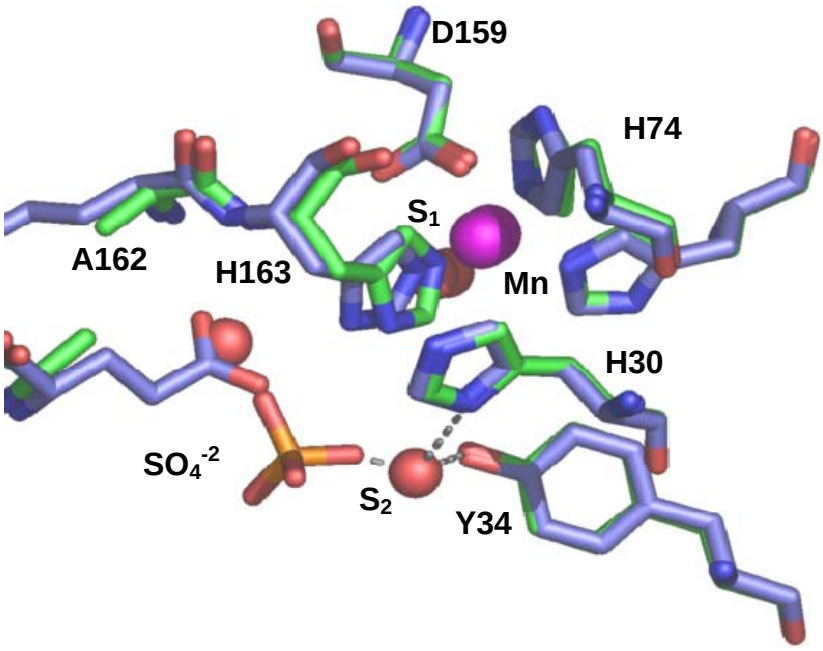

Figure 3-7 Structure of E162A MnSOD (shown in green) superimposed on wild-type human MnSOD (shown in blue) in the region of the mutated residue. Red spheres represent solvent and the manganese is shown in purple. In the mutant, a sulfate molecule was found bound near the position of the carboxyl group of Ala162 and in possible interaction with S2.

Discussion

Structures of E162D and E162A MnSOD

In wild-type MnSOD, the side-chain of Glu162 forms a hydrogen bond with the side chain of His163 from the adjacent subunit MnSOD (Borgstahl et al., 1992). This interaction is dampened in E162D MnSOD as the carboxyl group is more distant from

His163 by the length of one methylene group and by the intervention of a solvent molecule bridging Asp162 and His163 (Figure 3-6); however, the hydrogen bond to His163 is maintained through the intervening water molecule. This interaction is abolished in E162A MnSOD (Figure 3-7). As a result of the altered interaction between the side chains of residues 162 and 163, the coordination geometry is changed for E162A, though not so for E162D, presumably because a solvent molecule bridges the gap between Asp162 and His163. Another possible cause for the altered ligand distances for E162A may be the low metal occupancy (54%). The positions of other active-site residues His30, Tyr34, Gln143 are unaltered for either mutant.

An area of spurious density was observed surrounding Asp162 and Ala162 that was attributed to sulfate binding (Figures 3-6 and 3-7). Alignment of the sulfate-binding region of E162D and wild-type MnSOD indicates an opening of the structure. The solvent at position S_2 (Figure 3-1) is replaced by sulfate in the E162D structure. The sulfate-binding region of E162A shows hydrogen bonding of sulfate to the side chains of His30 and Tyr34. This could indicate a pathway for superoxide entry into the region of the active-site cavity. Sulfate was not present in measurements of catalysis or of spectral properties of these mutants of MnSOD although formate was used as a hydroxyl scavenger in pulse radiolysis experiments.

Differential scanning calorimetry showed that the main unfolding transition of E162D MnSOD (88^{o} C) is not significantly altered compared with wild-type human MnSOD (90^{o} C), consistent with the retention in the mutant of the hydrogen bond between Asp162 and His163 through an intervening water molecule. In contrast, this transition for E162A is decreased by 15^{o} C, attributed in significant part to the removal of

a stabilizing interaction with His163 from the adjacent subunit. The reduced stability, however, did not affect tetramerization of E162A.

Visible Spectroscopy

The visible spectrum of Mn^{3+}SOD is characterized by a broad absorption in the visible region with a maximum at 480 nm (Hearn et al., 1999; Bull and Fee, 1985). The pH profile of this maximum titrates with reported values of pK_a of 9.3 (Bull and Fee, 1985) and 9.7 (Maliekal et al., 2002) for *E. coli* MnSOD, and 9.4 (Guan et al., 1998) and 9.2 (this study) for the human MnSOD. Although there has been some disagreement as to the source of this ionization, a thorough study in *E. coli* MnSOD assigns this to Tyr34 (Maliekal et al., 2002), with corroborating evidence from Y34F that Tyr34 is also the source of this ionization in human MnSOD (Guan et al., 1998). NMR studies conducted on *E. coli* MnSOD showed that a pH-related chemical shift change corresponding to ionization of the phenolic hydroxyl of Tyr34 exhibited a pK_a of 9.5 ± 0.2 (Maliekal et al., 2002). Human Y34F MnSOD exhibits a pK_a near 11 significantly different than the visible spectrum of wild-type MnSOD (Hsu et al., 1996; Guan et al., 1998). Ionization of Tyr34 is also most likely the source of the $pK_a \sim 9.5$ in catalysis by human MnSOD (Bull and Fee, 1985; Hearn et al., 2001; Greenleaf et al., 2004).

The mutations E162D and E162A affect this critical pK_a in the visible spectrum of human MnSOD; however, this effect appears to shift the pK_a in opposite directions for each mutant (Figure 3-2). The change in this pK_a should be explained in terms of the effects of these mutations on the ionization of Tyr34. This comment does not preclude changes in the ionization of ligands of the metal, just that these appear to be outside of the pH range of these studies. Therefore, the changes in the pK_a of the visible absorption

are attributed to Tyr34, the side chain of which is located 6.2 Å from the carboxylate of Glu162 from the adjacent subunit in wild-type MnSOD. The crystal structures allow us to comment on the mutations at residue 162 on the ionization of Tyr34. His163 is within 3.3 Å of S_2 in the hydrogen-bond network, allowing indirect interaction between Glu162 and Tyr34 (Hearn et al., 2003; pdb accession #1LUV). The side chain of Asp162 in the E162D mutant maintains an interaction with Tyr34 through a solvent-bridged interaction with His163 while in E162A this interaction does not exist. Alteration of Glu162 could affect the ionization of Tyr34 through its altered or abolished interaction with His163. Understanding how Glu162 affects the ionization of Tyr34 warrants further study.

Catalysis

Replacement of the second-shell ligand Glu162 by Ala and Asp resulted in diminished catalysis in human MnSOD (Table 3-1). Though not essential for catalysis, mutation of Glu162 resulted in at least a five-fold decrease in rate constants k_1-k_3 for E162D and a 20-fold decrease for E162A. This is related to the diminished interaction between the Glu162 and His163 and the possible concomitant effects on the properties of the metal and active-site residues such as Tyr34. There is a precedent for substantial changes in catalysis with mutations at a second-shell ligand and at the dimeric interface.

Table 3-3 Maximal values for kcat/Km and k0/[E] for the catalysis of human wild-type MnSOD and mutants.

	K_{cat}/K_m (μM^{-1} sec^{-1})	$k_0/[E]$ (sec^{-1})
WT [b]	800	500
E162D[a]	290	270
E162A[a]	120	190
H30N [c]	130	2000
Y166F [d]	95	360

(a) 2mM TAPS pH 7.7, 50mM EDTA, 30 mM formate (see methods for pulse radiolysis)
(b) Ramilo et al., 1998
(c) Hearn et al., 2003
(d) Hearn et al., 2001

The replacement of the second-shell ligand Gln143 with Asn resulted in a 100-fold reduction in catalysis and evidence of an increase in the redox potential of the active site (Leveque et al., 2000; Hsieh et al., 1998). The mutation Y166F at the dimeric interface of human MnSOD resulted in a 10-fold decrease in catalysis (Hearn et al., 2004).

One interesting aspect of the catalysis k_1 and k_2 for the mutants at residue 162, as well as the step that forms the inhibited complex k_3 (Figure 3-4), is that they appear to have pH profiles similar to the titration of their visible spectra. E162D MnSOD showed a pH dependence for rate constants k_1-k_3 with values of kinetic pK_a from 8.0 to 8.7 that roughly matched the pK_a of the molar absorptivity (Figures 3-2, 3-4). This pH dependence was also evident in the values for k_{cat}/K_m (Figure 3-5). There was no observed pH dependence for the kinetic constants k_1-k_3 for E162A MnSOD in our pH range of 7.5 – 10.0, roughly consistent with its higher pK_a derived from the pH dependence of its visible spectrum. Presumably, the pH profiles for E162D and E162A are the result of the altered, indirect interaction between Glu162 and Tyr34. E162D MnSOD is the first reported variant of human MnSOD with a pH dependence that appears well within the range of practicable kinetic measurements and should be useful for further studies.

Comparison with MnSOD from *E. coli*

There have been rather few differences noted in k_1 and k_2 in catalysis between MnSOD from *E. coli* and humans; consequently, several differences revealed in this study warrant further attention. The mutant E162A human MnSOD retains specificity for manganese and is catalytically active although at about 5% the level of human wild type

(Table 3-1). Additionally, it remains a tetramer in solution. This is in contrast to the equivalent mutation in *E. coli*, E170A, which results in complete loss of catalytic activity, dimer destabilization in solution, and is accompanied by a change in specificity to $Fe^{2+/3+}$ (Whittaker and Whittaker, 1998) It is possible that measurement of catalysis for *E. coli* E170A was not sensitive enough to measure 20-fold decreased catalysis. In addition, the presence of a tetrameric interface in the E162A enzyme confers added stability not present in the *E. coli* E170A, thus the *E. coli* mutant is both monomeric and dimeric in solution. However, the retention of metal specificity is unique to the human E162A.

Comparison of the crystal structures of the human and *E. coli* forms of MnSOD shows nearly superimposable residues for the ligands of the metal and side chains Tyr34 and His30. However, there is a substructure of the active site that is considerably different for these two forms of MnSOD, and this offers significant clues to the different responses of the human and *E. coli* forms of MnSOD to replacements at residue 162. Specifically, described here are the structural features likely to account for the more extensive changes in *E. coli* MnSOD compared with human MnSOD upon mutation at 162 and estimate how these structural features might relate to activity and ionization of Tyr34. Included in the interactions that form the dimeric interface of MnSOD is a van der Waals interaction between Phe66 and Gln119 (3.5 Å) in the human enzyme (Quint and Reutzel et al., 2006; pdb # 1ADQ) and between Phe124 and Asn73 (4.0 Å) in *E. coli* (Edwards et al., 1998; pdb # 1VEW) (Figure 3-8). The orientations of these residues are similar in the *E. coli* enzyme though they are at a greater distance from each other compared to human MnSOD. In addition, Phe124 from the adjacent subunit in *E. coli* MnSOD interacts with Tyr34 (3.2 Å) in *E. coli* MnSOD. Dimeric destabilization of *E.*

coli E170A could alter this interaction with Tyr34 and thus affect ionization of the phenolic hydroxyl. The observations described here clarify differences in stability and in catalytic activity between the two enzymes, though they do not sufficiently address the altered metal selectivity exhibited by the two mutants, opening another avenue for future study.

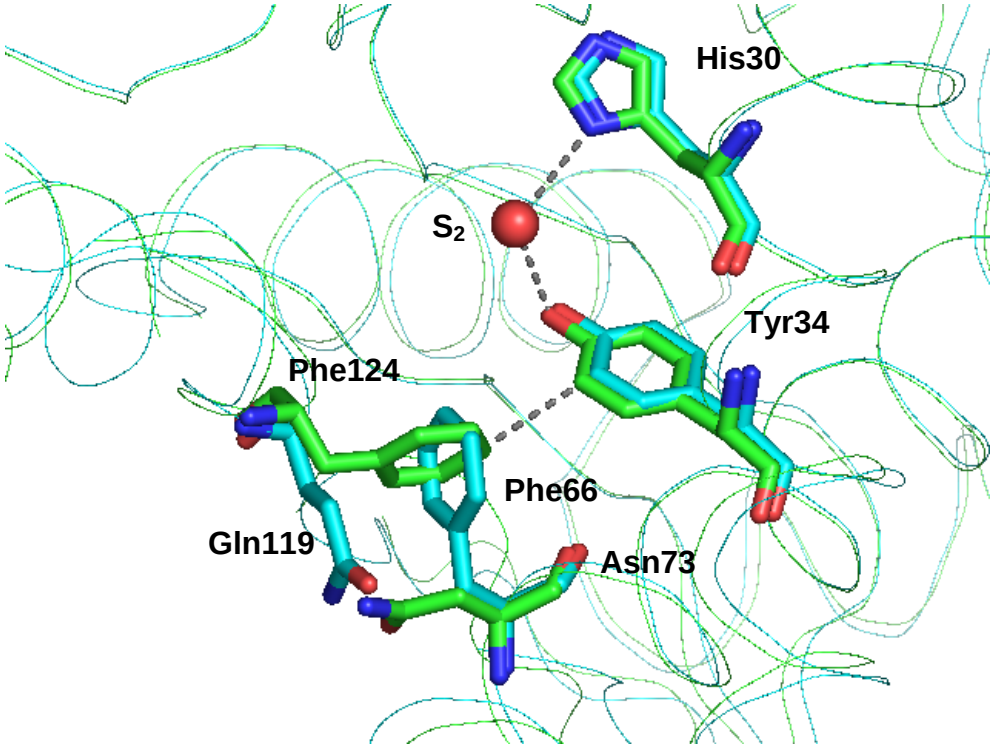

Figure 3-8 Structure of E. coli MnSOD (green) superimposed on wild-type human MnSOD (blue) in the dimeric interface. Red sphere represents S2 from the hydrogen-bond network. Shown is the interaction between Phe66 and Gln119 from the adjacent subunit (green). Also shown are Tyr34 and His30. Residues Phe124 and Asn73 (green) are shown for the E. coli enzyme with an interaction between Phe124 and Tyr34 denoted with a dotted line.

Product Inhibition

Product inhibition is a prominent feature of catalysis by human and *E. coli* MnSOD (Hearn et al., 2001). The rather significant decreases in k_1-k_4 describing catalysis and inhibition by E162D and E162A human MnSOD (Table 3-1), are similar to the observed zero-order component of catalysis. The maximal values of k_0/[E], the normalized, zero-

order rate constant for product inhibition, are similar for E162D, E162A, though diminished compared to wild-type MnSOD: 267 s^{-1}, 189 s^{-1}, and 500 s^{-1}, respectively (Table 3-3) (Hsu et al., 1996). For E162A, the value of $k_0/[E]$ was reduced to 20 s^{-1} at pH > 8.5 reflecting the pH dependence of k_4. The cause of the similar values of $k_0/[E]$ for E162D and E162A is due in significant part to the values of the ratio of k_2/k_3 in the two mutants (Table 3-1). This is a gating ratio that determines the extent of reaction that proceeds to catalysis versus inhibition (eq 3-2, 3-3), and the similar gating ratios for E162D and E162A are consistent with similar extents of product inhibition. The gating for wild-type human MnSOD is 1:1 while it is ~1:2 for both E162D and E162A (Table 3-1). This gating ratio is 5:1 for *E. coli* MnSOD (unpublished) (Table 3-1) indicating a less product-inhibited enzyme. This represents another key difference between human and *E. coli* MnSOD that warrants further study.

The side-chain of Glu162 is important for dissociation of the product-inhibited complex as evidenced by the similar values for k_4 for both E162A and E162D (Table 3-1) The E162A mutant is the only mutant of human MnSOD observed to date that has exhibited a pH related decrease in the value for k_4. This provides another avenue for future investigation since neither the structure of the inhibited complex nor its mechanism of dissociation is known. The values for k_4 do not follow the same pH dependence as k_1-k_3 because protonation of the bound peroxide is a different process from k_1-k_3 (Hearn et al., 2001).

CHAPTER 4
STRUCTURE OF NITRATED HUMAN MANGANESE SUPEROXIDE DISMUTASE

Introduction

The presence of nitrated proteins is associated with a number of pathological states (Ischiropoulos and Beckman, 2003; Radi, 2004; Shishehbor et al., 2003) and with certain diseases characterized by inflammatory processes (MacMillan-Crow et al., 2003). Human MnSOD in the presence of peroxynitrite is nitrated at a number of sites, but the observed near complete inhibition of catalysis is associated with the nitration of Tyr34 (Yamakura et al., 1998; MacMillan-Crow, Crow and Thompson, 1998; MacMillan-Crow and Thompson, 1999). Chapter 3 described the importance of the dimeric interfacial residue Glu162 and its role in supporting an important pK_a for catalysis through its interaction with Tyr34. Building on the findings of chapters three, the structure of nitrated human MnSOD was solved, emphasizing the importance of Tyr34 in catalysis and providing a structural explanation for peroxynitrite-mediated inactivation of MnSOD.

The side chain of Tyr34 plays an important role in catalysis. The replacement of Tyr34 with Phe causes minor effects on the catalytic efficiency (k_{cat}/K_m) of human and *E. coli* MnSOD (Guan et al., 1998; Whittaker and Whittaker, 1997); however, it does decrease by 10-fold the value of k_{cat} which determines the maximal velocity of catalysis (Guan et al., 1998). The crystal structure of the mutant human MnSOD with Phe34 is nearly identical to that of wild type, with Phe34 closely superimposed on the phenolic side chain of Tyr34 in the wild-type (Guan et al., 1998). Moreover, the replacement of

Tyr34 with Phe causes no significant change in the redox potential of the human enzyme (Leveque et al., 2001).

Nitration of tyrosine occurs through two possible mechanisms shown in figure 4-1.

$$^{\cdot}NO + O_2^{\cdot -} \leftrightarrows ONOO^- + H \leftrightarrows ONOOH \leftrightarrows [^{\cdot}NO_2 + {}^{\cdot}OH] \quad (1)$$

$$ONOO^- + CO_2 \leftrightarrows ONOOCO_2 \leftrightarrows [^{\cdot}NO_2 + CO_3^{\cdot -}] \quad (2)$$

nitrosoperoxycarbonate

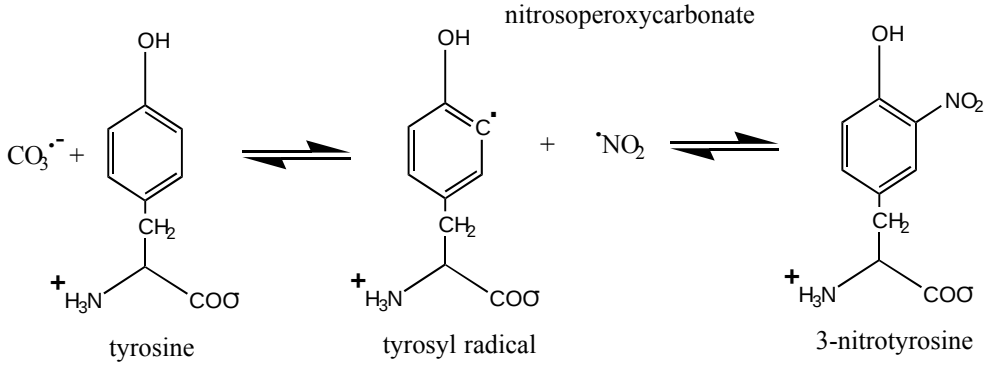

Figure 4-1 Scheme for nitration of tyrosine in the presence of peroxynitrite showing nitration through the pathway of equation 2.

Nitration of biomolecules by peroxynitrite is enhanced by the presence of CO_2 with the reaction of equation 2 predominating over the reaction of equation 3. Production of carbonate radical promotes tyrosyl formation and subsequent reaction with $^{\cdot}NO_2$ yields 3-nitrotyrosine (Figure 4-1) (Bonini et al., 1999). Nitration of tyrosine 34 in MnSOD is associated with abolished activity.

The X-ray crystal structure of nitrated wild-type human MnSOD, as well as the unmodified enzyme, were both resolved to 2.4 Å resolution. Although mass spectrometry detected partial nitration of several tyrosines and a tryptophan near the surface of the protein, the crystal structure shows only nitration of Tyr34 in the active site. This nitrated side chain, 3-nitrotyrosine 34, exhibited only one conformer with the nitro group extending toward the metal-bound hydroxide/water but not forming a hydrogen bond with it. Instead the O1 of the nitro group appears to form a hydrogen bond with the Nε2 of residue Gln143. The structure of the nitrated enzyme including active-site residues and

the phenyl ring of 3-nitrotyrosine 34 are closely superimposable with the unmodified wild-type MnSOD. The conformation in the active-site cavity of the nitrated MnSOD strongly suggests inhibition by steric interference, by a possible weakening of a hydrogen bond network, and by the electrostatic effects related to the presence of the nitro group and the resulting change of the redox potential.

Materials and Methods

Preparation of Nitrated Human MnSOD

Peroxynitrite was produced by mixing equal volumes (5 ml) of $NaNO_2$ (0.8 M) and acidified H_2O_2 (0.7 M H_2O_2 and 0.3 M HCl) in a manually operated dual-syringe mixer and quickly quenched with (3 ml) 3 M NaOH (Crow, Beckman and McCord, 1995). The final solution was purified using a MnO_2 gravity column to remove excess H_2O_2 and a subsequent Chelex 100 gravity column to remove extraneous metal ions. The concentration of peroxynitrite was determined by measuring optical density at 302 nm (ε_{302} = 1670 M^{-1} cm^{-1}) (Hughes and Nicklin, 1968). The nitration of human MnSOD was carried out by the bolus addition of peroxynitrite to MnSOD in the presence of CO_2/HCO_3^-. MnSOD samples were equilibrated overnight at 4^oC prior to reaction with peroxynitrite. The mixed solution contained MnSOD (50 μM), all species of CO_2 (25 mM), peroxynitrite (8 mM), and phosphate buffer (20 mM) at pH 7.8 and 25^o C. Following reaction with peroxynitrite, samples of modified enzyme were pooled and concentrated in 20 mM phosphate pH 7.8.

Modified enzyme was digested with acetylated trypsin for 3 hours at 37^o C. Capillary reverse phase HPLC separation of tryptic fragments was performed on a PepMap C18 column (LC Packings, San Francisco, CA) in combination with an Ultimate

Capillary HPLC System (LC Packings, San Francisco, CA) operated at a flow rate of 200 nL/min. Extent of nitration was measured using a QSTAR XL (LC/MS/MS system, MDS Sciex, Ontario, Canada). To determine the ratio of nitrated versus unmodified MnSOD, the peak areas for modified and unmodified masses were compared. We determined the following extents of nitration: 75% nitration of Tyr34, 36% overall nitration of Tyr9 and Tyr11 (residues 9 and 11 were in the same tryptic fragment), 46% overall nitration of Trp180 and Trp186 (residues 180 and 186 were also in the same tryptic fragment).

Crystallization

Wild-type and nitrated human MnSOD were buffer exchanged into 20 mM phosphate buffer at pH 7.8 and concentrated (16 mg/ml) using a centricon YM-10 (Amicon). The samples were crystallized using the hanging drop vapor diffusion method (McPherson, 1982). The drops consisted of 5 μl of enzyme mixed with 5 μl of precipitant solution (3 M ammonium phosphate, 100 mM imidazole, 100 mM malate) and suspended over 1 ml of precipitant solution at 25^{o} C. The crystals grew to full size (0.8 x 0.5 x 0.5 mm) in approximately one week.

Data Collection and Processing

Both wild-type and nitrated human MnSOD X-ray diffraction data were collected from single crystals, wet mounted in quartz capillaries (Hampton Research), on an R-AXIS IV++ image plate (IP) system with Osmic mirrors and a Rigaku HU-H3R CU rotating anode operating at 50 kV and 100 mA (Rigaku/MSC). A 0.3 mm collimator was used with a crystal to IP distance of 220 mm and the 2θ angle fixed at 0^{o}. The frames were collected using a 0.3^{o} oscillation angle with an exposure time of 5 min/frame at room temperature. Both data sets were indexed using DENZO and scaled and reduced

with SCALEPACK software (Otwinowski and Minor, 1997). Diffraction intensities were visible to 2.4 Å resolution and a total of 200 frames were collected from both wild type and nitrated human MnSOD crystals.

Structure Determination and Refinement

To prevent any model phase bias, the initial phasing model for both the unmodified and nitrated human MnSOD was the structure of the W161A MnSOD mutant (Hearn et al. 2001; pdb accession number 1JA8) from which the nine tyrosines (residues: 9, 11, 34, 45, 165, 166, 169, 176, and 193) and six tryptophans (residues: 78, 123, 126, 161, 181, and 186) had been replaced by alanines, and the Mn^{2+} ion and solvent molecules had been removed. The structures were phased and refined using the software package CNS (Brunger et al., 1998). Refinement cycling (using rigid body, simulated annealing (for the first cycle), minimization, and individual B-factor refinement) was interspersed with rounds of manual model building using the molecular graphics program O (Jones et al., 1991). Following the first cycle of refinement, the positions of the manganese ion, nine tyrosines, and six tryptophans were clearly identified and built into F_o-F_c electron density maps for both structures. After the second cycle of refinement the unambiguous electron density for a nitro group was observed in the vicinity of the Cε1 atom of tyrosine 34 for the nitrated human MnSOD and a model for a 3-nitrotyrosine residue was built and energy minimized using the PRODRG2 server (Schuettelkopf and Aalten, 2004) and placed into the electron density. The mass spectrometric analysis had previously determined the extent of Tyr 34 nitration to be ~75 %. Due to this observation, the atoms comprising the nitro group were refined with an occupancy of 0.75 compared to the rest of the atoms in the protein and solvent. Both structures were further refined for several more cycles with some minor manual building, after which solvent molecules were

picked both automatically in CNS (using a 3 sigma cut off) and manually in O by inspection of F_o-F_c electron density maps. The bond geometry of the models was analyzed using the software package PROCHECK (Laskowski et al., 1993). The final, refined models and structure factor files have been deposited with the Protein Data Bank, PDB (accession codes 2ADQ, and 2ADP for the unmodified and nitrated human MnSOD, respectively).

Results

The structures of the unmodified and the nitrated human wild-type MnSOD have been solved in the hexagonal space group $P6_122$, with unit cell parameters a = b = 81.3 and c = 242.2 Å, and refined to 2.4 Å resolution (Table 4-1, Supplementary material 1 and 2). The final refined structure of the unmodified human MnSOD had an R_{cryst} of 21.7 % (R_{free} of 24.0 %) with an average B-factor of 26.2 $Å^2$; and the nitrated human MnSOD had an R_{cryst} of 19.7% (R_{free} of 21.8 %) with an average B-factor of 31.2 $Å^2$ (Table 4-1). Following the second cycle of refinement the position of a single 3-nitrotyrosine 34 was built into F_o-F_c and 2 F_o-F_c electron density maps in the nitrated human MnSOD structure (Figure 4-2). The occupancy for the nitro group on 3-nityrosine34 was modified to reflect the percent nitration determined by mass spectrometry. There was no unique density surrounding tyrosines 9 and 11 or tryptophans 181 and 186.

A comparison of the wild-type and nitrated human MnSOD structures showed no significant side-chain conformational changes or solvent displacement in the active site with the nitration of tyrosine 34 (Figure 4-3). The root-mean-squared difference for all C_α atoms was 0.13 Å comparing the nitrated with unmodified MnSOD. The active-site

manganese of wild-type human MnSOD has been previously reported (Borgstahl et al., 1992) as coordinated by the Nε2 of three histidine residues (H26, H74, H163), Oδ1 of Asp159, and a Mn bound water/hydroxide molecule arranged in a distorted trigonal bipyramidal geometry. The nitration of Tyr34 caused no significant change in this geometry or in first shell ligand distances (Figure 4-2). Also of interest was that the overall refined thermal individual atom B values for both structures were similar and there was no significant difference for the manganese in unmodified and nitrated human MnSOD with values of 16.9 and 21.6 $Å^2$, respectively. Of note, which may or may not be of significance, was the B values for the Mn bound water/hydroxide molecule which was 11.6 $Å^2$ for wild-type and nearly twice the value 19.1 $Å^2$ for nitrated human MnSOD. The significance of this can only be resolved with either higher resolution X-ray diffraction data or a neutron diffraction structure.

In comparing the crystal structures of the nitrated and unmodified wild-type human MnSOD, we observed that the side chain of 3-nitrotyrosine 34 was in a single side-chain conformer with the O1 and O2 positioned 3.6 and 3.8 Å from the manganese ion. Probably the most significant interaction observed by the nitration of Tyr34 is the inferred hydrogen bond (3.1 Å) between O1 of 3-nitrotyrosine 34 and Nε2 of Gln143 (Table 4-2, Figure 4-3).

A comparison of the two non-crystallographic subunits of the human nitrated MnSOD in the hexagonal space group $P6_122$ (data not shown) showed no differences in orientation of the nitrated Tyr34 residues and they were subsequently averaged in the refinement protocols. There was also no evidence of dityrosine (3,3'-dityrosine) formation in the crystal structure.

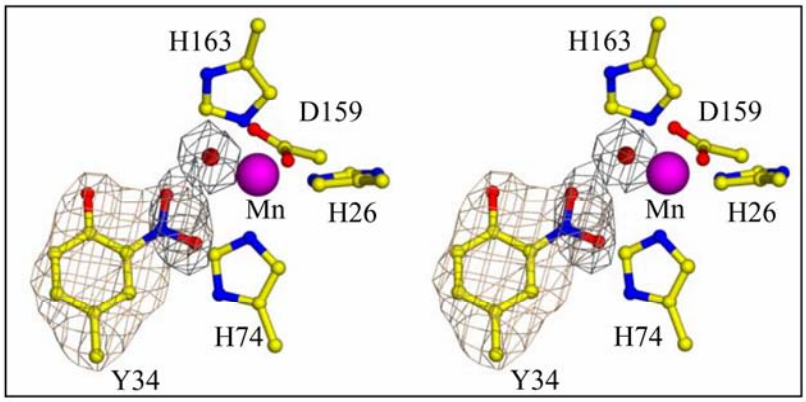

Figure 4-2 Structure of the active site of the nitrated human MnSOD. Stereo diagram showing the initial, no model bias (F_o-F_c) and ($2F_o$-F_c) electron density maps contoured at 3.0 σ (black) and 1.0 σ (grey), respectively, into which the 3-nitrotyrosine 34 and manganese-bound hydroxide were modeled. The active site manganese (pink) is pentacoordinate with inner shell ligands His26, His74, His163, Asp159, and the metal-bound solvent molecule.

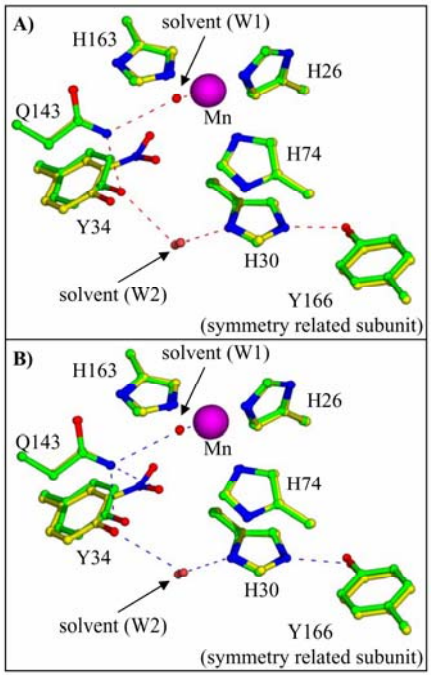

Figure 4-3 The structure of the active-site region of nitrated (yellow) superimposed onto unmodified human MnSOD (green). A) The proposed hydrogen bond network (red dashed lines) for unmodified wild type, and B) the proposed hydrogen bond network (blue dashed lines) for nitrated human MnSOD. The proposed hydrogen bond network involves residues Gln143, Tyr34, His30, solvent molecule (W2) and Tyr166. See Table 4-2 for a complete listing of distance geometry.

Table 4-1 X-ray crystallographic structure statistics of unmodified and nitrated human MnSOD

	Unmodified	Nitrated
Data Collection		
Resolution (Å)	20.0-2.4 (2.49-2.4)*	20.0-2.4 (2.49-2.4)
Space group	$P6_122$	$P6_122$
Unit cell (Å)	a=b=81.3, c=242.2	*a*=*b*=81.3, *c*=242.2
Molecules/a.s.u.	2	2
[a]R_{sym} (%)	10.2 (19.1)	10.9 (14.9)
Reflections (total/unique)	244,364 / 61,091	231,776 / 60,459
Completeness (%)	95.8 (90.2)	91.3 (80.6)
Refinement		
Non-hydrogen atoms	1629	1605
Water molecules	74	46
Average B factors (Å^2)		
Protein main-chain	25.1	30
Protein side-chain	27.2	32.3
Solvent molecules	35.9	36.8
Tyrosine 34	20.3	27.6
R_{cryst}/R_{free} (%)	21.7 / 24.0	19.7 / 21.8
R.m.s.d bond lengths (Å) /angles (^{o})	0.006 / 1.3	0.006 / 1.3

*Data for the highest resolution shell are given in parentheses.
[a]$R_{sym} = \Sigma |I-\langle I\rangle| / \Sigma I \times 100$, where I is the intensity of a reflection and <I> is the average intensity.
[b]$R_{cryst} = \Sigma_{hkl} |F_o-KF_c| / \Sigma_{hkl} |F_o| \times 100$, R_{free} is calculated from 5% randomly selected data for cross-validation.
[c]R.m.s.d. = root mean square deviation.

The nitration at Tyr9 and 11 was less extensive (36% overall) and was not observed in the crystal structure; mobility of these surface residues may have made the nitration less evident. Nitration at Trp180 and 186 was also not observed in the crystal structure.

Discussion

The structure of human MnSOD containing 3-nitrotyrosine at position 34 is well-defined by the 2.4 Å electron density map (Figure 4-1) with a three-dimensional structure closely superimposable with the unmodified enzyme (Figure 4-2); specifically, there are

no conformational changes in the active-site cavity. This is the first reported crystal structure of a nitrated MnSOD, to our knowledge.

Table 4-2 Distance geometries (Å) in the active-sites of unmodified and nitrated human MnSOD

Interaction		Wild-type	Nitrated
Mn^{2+}	[a]Solvent W1	2.1	2.1
[a]Solvent W1	Q143-Nε2	3.1	3.1
Q143-Nε2	Y34-OH	2.5	3.1
Y34-OH	[a]Solvent W2	3.1	3.3
[a]Solvent W1	Y34-O1	---	3.5
Q143-Nε2	Y34-O1	---	3.1
Y34-O1	Mn^{2+}	---	3.6
Y34-O2	Mn^{2+}	---	3.8
[a]Solvent W2	H30-Nδ1	2.9	3.0
H30-Nε2	Y166-OH	2.6	2.6

[a]See figure 4-2 for position of solvent W1 and W2.

The nitrated Tyr34 side chain shows only a single conformer with the nitro group directed toward the metal (Figure 4-1). This conformer predominates in large part because of electrostatic gradients within the active-site cavity as discussed below; however, there are probably also steric considerations that limit the range of side-chain conformations of nitrated Tyr34. For example, the side chain of Phe66 is within 3.6 Å of that of 3-nitrotyrosine 34 and limits the range of orientations of this nitrated residue. In addition, there is a role for manganese in the reaction of MnSOD with peroxynitrite (Quijano et al., 2001); hence, the orientation of 3-nitrotyrosine in the nitrated enzyme may reflect the reactive site of the side chain of Tyr34 that is closest to the metal.

Although the nitro group of modified Tyr34 is near the manganese bound hydroxyl/water, the distance between oxygen atoms at 3.5 Å (Table 4-2) is too great to form a hydrogen bond, nor is the nitro group sufficiently close, ~3.7 Å, to the metal to be considered an inner shell ligand. The nitro group is viewed more accurately as a second-

shell ligand of the manganese, although its presence causes no changes in geometry or distances of the first-shell ligands. However, the crystal structure is consistent with a hydrogen bond between the nitro group at Tyr34 and the Nε2 of Gln143, with a distance of 3.1 Å from the O1 of nitrated-Tyr34. There is still evidence for a hydrogen bond between the Nε2 of Gln143 and the phenolic OH of nitrated-Tyr34 with a distance of 3.1 Å (Table 4-2, Figure 4-2). However, this distance is considerably lengthened compared with that of the unmodified enzyme and this hydrogen bond involving Nε2 of Gln143 may be bifurcated between the phenolic OH and the nitro group of 3-nitrotyrosine 34.

Nitration of human MnSOD inhibits catalysis by greater than 90% (Yamakura et al., 1998; MacMillan-Crow et al., 1998). This inhibition is associated with nitration of Tyr34 (Yamakura et al., 1998; MacMillan-Crow et al., 1998), although there is evidence that nitration of other tyrosine residues may also decrease activity (MacMillan-Crow et al., 1999). We comment then on the likely causes of inhibition by MnSOD containing 3-nitrotyrosine at position 34. First, it appears that nitration has not affected the stereochemistry of the active site residues; that is, the conformation of Gln143, which forms a hydrogen bond with the aqueous ligand of the metal, is not altered and the side-chain orientation of Tyr34, although nitrated, is not changed. So conformational changes induced by nitration are not pertinent in the inhibition. However, the hydrogen bond network involving the side chains of Gln143, Tyr34, His30, and Tyr166 from an adjacent subunit appears to be altered and possibly weakened at 3-nitrotyrosine (Table 4-2, Figure 4-2), as mentioned above. This network, and particularly Tyr34, has been associated with proton transfer in catalysis by wild-type MnSOD, either proton transfer to product peroxide or to the metal-bound hydroxide (Whittaker and Whittaker, 1997; Silverman

and Nick, 2002; Hunter et al., 1997; Sorkin, Duong and Miller, 1997; Bull and Fee, 1985; Stallings et al., 1991), and alteration of this network in the nitrated enzyme is consistent with inhibition.

Another likely cause of inhibition is simply that the bulk of the nitrated side chain inhibits catalysis, perhaps by its presence in the substrate access channel and/or steric overlap with the enzyme-substrate complex or with the transition state. This was the case with H30V MnSOD in which the C of Val30 is 4.4 Å from the manganese and either blocks the substrate access channel or has a steric overlap with the developing transition state. The O1 and O2 of the nitro group of nitrated Tyr34 are closer to the metal (near 3.7 Å) and also lie along a likely substrate access channel. The substrate access channel in MnSOD and FeSOD is exceedingly narrow and there is evidence from dynamics simulations that substrate diffusion to the vicinity of the manganese requires conformational fluctuations along this channel (Sines et al., 1990). A prominent side chain, the motion of which can open this channel, is Tyr 34 (Sines et al., 1990). Chemical modification by nitration of the phenolic side chain would certainly slow this process.

Yet another possibility for inhibition is the change in pK_a of nitrated Tyr, which is expected to be lower by about 2 pK_a units compared with unmodified Tyr. We have no measure of the pK_a of nitrated Tyr34 in MnSOD, although this value was estimated from spectroscopic data at pK_a 7.95 for FeSOD nitrated at Tyr34 (Soulere, 2001). Nitrated tyrosine would have a larger fraction as tyrosinate anion than unmodified, and could decrease catalysis by electrostatic repulsion of the substrate $O^{\bullet -}$ as well as have a major effect on the redox potential of the enzyme (Miller et al., 2003). The active-sites of MnSOD and FeSOD are very finely tuned to catalyze both the oxidative and reductive

stages of catalysis (Vance and Miller, 1998), and introduction of a nitro group near the metal is likely to alter this tuning. That is, the nitration of Tyr 34 has almost certainly altered the redox potential.

This study provides a connection between the nitration and subsequent inhibition of MnSOD. The location in the active site of the NO_2 group of 3-nitrotyrosine 34 gives a basis for understanding the strong inhibition of this essential antioxidant enzyme. It is notable that replacement of Tyr34 with Phe has very little effect on catalysis up to low micromolar concentrations of $O_2^{\bullet -}$ (Guan et al., 1998; Whittaker and Whittaker, 1997) and does not decrease thermal stability or alter the crystal structure (Guan et al., 1998). Yet its prominence in the active-site cavity makes it a site for nitration and inhibition of MnSOD.

CHAPTER 5
CONCLUSIONS AND FUTURE DIRECTIONS

Conclusions

This dissertation focused on the two structurally unique interfaces of human MnSOD. The overall goal was to understand the contributions to stability and catalysis of the two interfaces and to compare the tetrameric human MnSOD to the dimeric *E. coli* MnSOD. The data presented in chapters 2 and 3 of this study suggest that the tetrameric interface provides stability while dimeric interfacial residues play a greater role in catalysis. The importance of Tyr34 in maintaining catalysis was explored in chapter 4 with a structure of nitrated human MnSOD.

The Tetrameric Interface in Human MnSOD

One key characteristic of human MnSOD that differentiates it from *E. coli* is the presence of a tetrameric interface. Chapter 2 presented ^{19}F NMR and differential scanning calorimetry studies elucidating the roles of the two interfaces of human MnSOD and the data suggest a stabilizing role for the tetrameric interface. Though the tetrameric interface is generally associated with higher organisms, it may in fact be a more primitive structural arrangement. The endosymbiotic theory suggests a bacterial origin for mitochondria; perhaps mitochondria resulted from phagocytosis by a much larger cell billions of years ago. MnSOD may have originally been a tetramer to accommodate a higher average temperature caused by increased atmospheric CO_2 levels. As atmospheric CO_2 levels waned in the presence of photosynthesizing cyanobacteria, prokaryotes and eukaryotes diverged and the mitochondrion became a selective advantage for eukaryotes.

It is interesting that some heat extremophiles, like *T. thermophillus* and *P. aerophilus* utilize tetrameric MnSODs (Wagner et al., 1993; Whittaker and Whittaker, 2000).

The Dimeric Interface and Differential Roles of Glu162 in Human MnSOD and Glu170 in *E. coli* MnSOD

Considering the importance of the dimeric interface in stability and catalysis, chapter 3 emphasized the contribution to stability and catalysis of Glu162 in human MnSOD and Glu170 in *E. coli* MnSOD. In addition to an observed decrease in catalysis and altered product inhibition, E162D exhibited a pH dependence for catalysis not observed in the native enzyme. This observed pK_a for catalysis may be the result of an altered interaction with Tyr34 through His163 and a bridging solvent molecule. The E162A mutant is less stable, though it is still tetrameric in solution and is associated with a significantly diminished catalysis for the enzyme, emphasizing the importance of Glu162 in supporting catalysis and stabilizing the enzyme. In contrast, the equivalent mutation in the *E. coli* MnSOD, Glu170Ala, exhibits no activity, is selective for iron over manganese is a mixture of monomer and dimer in solution. This represents a significant difference between human and *E. coli* MnSOD, the active sites of which are structurally equivalent. A stabilizing interaction between Phe66 and Gln119 in the dimeric interface of human MnSOD is absent in the *E. coli* enzyme, thus the E170A mutant destabilizes to a greater extent than E162A. In addition, an interaction between Phe124 and Tyr34 exists in the *E. coli* MnSOD that is not present in the human enzyme. This could affect ionization of Tyr34 for the *E. coli* enzyme and perhaps affect its metal selectivity, though the latter remains an area for further research.

A Structural Explanation for Abolished Catalysis of Nitrated Human MnSOD

To add to a growing literature on the reaction of peroxynitrite with MnSOD, chapter 4 presented a structural explanation for abolished catalysis resulting from nitration of Tyr34. Previous studies have shown that nitration of Tyr34 is associated with complete catalytic inhibition (MacMillan-Crow et al., 1995) (Yamakura et al., 1996). The structure of nitro-MnSOD indicates that diminished catalysis is the result of steric blockade of the substrate as well as possible electrostatic repulsion of superoxide anion. These findings will help elucidate the role of nitro-MnSOD in certain diseases involving peroxynitrite-mediated nitration of biomolecules.

Future Directions

The Dimeric Interface of Human MnSOD

The peaks corresponding to fluorine labeled tyrosines shown in chapter 2 were significantly broad and four of the nine fluorine labeled tyrosines were not observed in the fluorine NMR spectrum (Figure 2-2). The peaks for Tyr34, Tyr165, Tyr166 and Tyr176 were not observed and may have been broadened due to their proximity to the paramagnetic manganese of the active site; all four tyrosines that were not observed are within 10 Å of the active site metal. One way to alleviate this problem would be to construct an apo-fluoro-MnSOD. This would involve expression and subsequent chelation of the metal from fluoro-MnSOD. The manganese is tightly bound in the active site and chelating the metal would involve denaturation and refolding of the enzyme. Initial attempts to chelate the manganese have resulted in an unfolded enzyme. Further attempts may involve the use of other chelators and perhaps changes in pH. Expression with a non-paramagnetic metal substitute may also alleviate the issue of excessively broadened lines.

Redox properties of E162 mutants

Measurement of redox properties of human MnSOD are difficult due to the size of the active site and require an electron mediator to measure the redox potential (Leveque et al., 2001). Mediators including ferricyanide and pentacyanoaminoferrate have been used successfully though the effective range of study is limited; to use ferricyanide, the midpoint potential for the enzyme must be below 435 mV. The cause of reduced catalysis in mutants E162A and E162D is not fully understood and measurement of the redox potential of E162D and E162A MnSOD may elucidate these causes.

Catalytic Properties of Nitrated MnSOD

Indirect studies (including xanthine oxidase assays) have shown that nitration of MnSOD abolishes activity of MnSOD. Direct methods like stopped-flow and pulse radiolysis have not been used to measure catalysis of nitro-MnSOD, in part because it is difficult to achieve 100% nitration of MnSOD. Catalytic studies could provide a more thorough explanation for catalytic decrease. Chapter 4 described the structure of nitrated MnSOD comprised of 74% nitration of Ty34. A pulse radiolysis study would require the purification of 100% nitrated enzyme using affinity chromatography. It would be interesting to determine rate constants k_1-k_4 for fully nitrated enzyme to see how nitration has altered catalysis of MnSOD. For instance, the enzyme could quickly enter a product inhibited state from which it does not dissociate.

Future of Therapeutic Studies

The potential for human MnSOD in drug discovery is great and future therapeautic studies will focus on the dimeric interface. For example, MnSOD mutants that are less product-inhibited, such as H30N, are useful as anti-proliferative agents (Davis et al., 2004) and could potentially be used as life-saving therapies during

reperfusion injury. In addition, the presence of nitrated MnSOD will serve as a biomarker for chronic diseases such as allograft rejection and could potentially be used as markers for cancer.

LIST OF REFERENCES

Ayala I., Perry, J. J. P., Szczepanski, J., Tainer, J. A., Vala, M.T., Nick, H.S., Silverman D.N. (2005) Hydrogen Bonding in Human Manganese Superoxide Dismutase Containing 3-Fluorotyrosine, *Biophysical J.* **89,** 4171-4179.

Barondeau, D. P., Kassmann, C. J., Bruns, C. K., Tainer, J. A., and Getzoff, E. D. (2004) Nickel superoxide dismutase structure and mechanism, *Biochemistry* **43**, 8038-47.

Beckman, J. S., Beckman, T. W., Chen, J., Marshall, P. A., and Freeman, B. A. (1990) Apparent hydroxyl radical production by peroxynitrite: implications for endothelial injury from nitric oxide and superoxide, *Proc. Natl. Acad. Sci. U S A* **87**, 1620-1624.

Beckman, J. S., Ischiropoulos, H., Zhu, L., van der Woerd, M., Smith, C., Chen, J., Harrison, J., Martin, J. C., Tsai, M. (1992) Kinetics of superoxide dismutase and iron-catalyzed nitration of phenolics by peroxynitrite. *Arch. Biochem. Biophys*. **298**, 438-445.

Becker, L. B. (2004) New concepts in reactive oxygen species and cardiovascular reperfusion physiology, *Cardiovascular Res.* **61**, 461-470.

Bondi, A., J. (1964) van der Waals volumes and radii. *Phys. Chem.* **68,** 441-451.

Bonini, M. G., Radi, R., Ferrer-Sueta, G., Ferreira, A. M., and Augusto, O. (1999) Direct EPR detection of the carbonate radical anion produced from peroxynitrite and carbon dioxide, *J. Biol. Chem.* **274**, 10802-10806.

Borgstahl, G. E., Parge, H. E., Hickey, M. J., Beyer, W. F., Hallewell, R. A., Tainer, J. A. (1992) The Structure of Human Mitochondrial Manganese Superoxide Dismutase Reveals a Novel Tetrameric Interface of Two 4-Helix Bundles, *Cell,* **71**, 107-118.

Borgstahl, G. E., Parge, H. E., Hickey, M. J., Johnson, M. J., Boissinot, M., Hallewell, R. A., Lepock, J. R., Cabelli, D. E., and Tainer, J. A. (1996) Human mitochondrial manganese superoxide dismutase polymorphic variant Ile58Thr reduces activity by destabilizing the tetrameric interface, *Biochemistry* **35**, 4287-4297.

Borgstahl, G. E., Parge, H. E., Hickey, M. J., Jr Beyer, W. F., Hallewell, R. A., Tainer, J. A. (1992) The structure of human mitochondrial manganese superoxide dismutase reveals a novel tetrameric interface of two 4-helix bundles. *Cell* **71,** 107-118.

Brunger, A. T., Adams, P. D., Clore, G. M., DeLano, W. L., Gros, P., Grosse-Kunstleve, R. W., Jiang, J. S., Kuszewski, J., Nilges, M., Pannu, N. S., Read, R. J., Rice, L. M., Simonson, T., Warren, G. L. (1998) Crystallography & NMR system: A new software suite for macromolecular structure determination, *Acta Crystallogr D Biol Crystallogr.* **54**, 905-921.

Bull, C. A. and Fee, J. A. (1985) Steady-state kinetics of superoxide dismutases: properties of the iron containing protein from *Escherichia coli*, *J. Am. Chem. Soc.* **107**, 3295-3304.

Bull, N., Yoshida, Fee (1991) Kinetic studies of superoxide dismutases: properties of the manganese-containing protein from Thermus thermophilus, *J. Am. Chem. Soc* **113**, 4069-4076.

Cabelli, D. E., Guan, Y., Leveque, V., Hearn, A. S., Tainer, J. A., Nick, H. S., Silverman, D. N. (1999) Role of tryptophan 161 in catalysis by human manganese superoxide dismutase, *Biochemistry* **38**, 11686-11692.

Chalmers, M.J., Busby, S.A., Pascal, B.D., He, Y., Hendrickson, C.L., Marshall, A.G. and Griffin, P.R. (in press) Probing protein ligand interactions by automated hydrogen/deuterium exchange mass spectrometry. *Anal. Chem*.

Choudhury, S. B., Lee, J. W., Davidson, G., Yim, Y. I., Bose, K., Sharma, M. L., Kang, S. O., Cabelli, D. E., Maroney, M. J. (1999) Examination of the nickel site structure and reaction mechanism in Streptomyces seoulensis superoxide dismutase, *Biochemistry* **38**, 3744-3752.

Crow, J.P., Beckman, J.S., McCord, J.M. (1995) Sensitivity of the essential zinc-thiolate moiety of yeast alcohol dehydrogenase to hypochlorite and peroxynitrite. *Biochemistry*. **34**, 3544-3552.

Delano W. L. (2002) The PyMOL User's Manual San Carlos, CA: DeLano Scientific; last accessed June 2006, http://www.pymol.org**.**

Denicola, A., Freeman., BA, Trujillo., M, Radi, R. (1996) Peroxynitrite reaction with carbon dioxide/bicarbonate: kinetics and influence on peroxynitrite-mediated oxidations. *Arch Biochem. Biophys.* **333**, 49-58.

Edwards, R. A., Baker, H.M.,Whittaker, M.M., Whittaker, J.W., Jameson, G.B., Baker, E.N. (1998) Crystal Structure of Escherichia coli manganese superoxide dismutase at 2.1-angstrom resolution, *J. Biol. Inorg. Chem* 3, 161-171.

Emsley, P., and Cowtan, K. (2004) Coot: model-building tools for molecular graphics, *Acta. Crystallogr. D Biol. Crystallogr.* **60**, 2126-2132.

Fridovich, I. (1989) Superoxide dismutases. An adaptation to a paramagnetic gas, *J. Biol. Chem.* **264**, 7761-7764.

Fridovich, I. (1995) Superoxide radical and superoxide dismutases. *Annual Reviews of Biochemistry* **64**, 97-112.

Greenleaf, W. B., Perry, J. J., Hearn, A. S., Cabelli, D. E., Lepock, J. R., Stroupe, M. E., Tainer, J. A., Nick, H. S., and Silverman, D. N. (2004) Role of hydrogen bonding in the active site of human manganese superoxide dismutase, *Biochemistry* **43**, 7038-45.

Groves, J. T. (1999) Peroxynitrite: Reactive, Invasive and Enigmatic *Curr. Opinion in Chem. Biol.* **3**, 226-235.

Guan, Y., Hickey, M. J., Borgstahl, G. E., Hallewell, R. A., Lepock, J. R., O'Connor, D., Hsieh, Y., Nick, H. S., Silverman, D. N., and Tainer, J. A. (1998) Crystal structure of Y34F mutant human mitochondrial manganese superoxide dismutase and the functional role of tyrosine 34, *Biochemistry* **37**, 4722-30.

Harman, D. (1956).Aging: a theory based on free radical and radiation chemistry, *Journal of Gerontology* **11**, 298-300.

Haber, F., Weiss, J. (1934) The catalytic decomposition of hydrogen peroxide by iron salts, *Proc. Roy. Soc.* **147,** 332-351.

Halliwell, B. (1995) Oxygen radicals, nitric oxide and human inflammatory joint disease, *Ann. Rheum. Dis.* **54**, 505-10.

Hearn, A. S., Fan L., Lepock, J. R., Luba, J. P., Greenleaf, W. B., Cabelli, D. E., Tainer, J. A., Nick, H. S., Silverman, D. N. (2004) Amino acid substitution at the dimeric interface of human manganese superoxide dismutase, *J. Biol. Chem* **279**, 5861-5866.

Hearn, A. S., Stroupe, M. E., Cabelli, D. E., Lepock, J. R., Tainer, J. A., Nick, H. S., and Silverman, D. N. (2001) Kinetic analysis of product inhibition in human manganese superoxide dismutase, *Biochemistry* 40, 12051-8.

Hearn, A. S., Stroupe, M. E., Cabelli, D. E., Ramilo, C. A., Luba, J. P., Tainer, J. A., Nick, H. S., and Silverman, D. N. (2003) Catalytic and structural effects of amino acid substitution at histidine 30 in human manganese superoxide dismutase: insertion of valine C gamma into the substrate access channel, *Biochemistry* **42**, 2781-9.

Hearn, A. S., Tu, C., Nick, H. S., and Silverman, D. N. (1999) Characterization of the product-inhibited complex in catalysis by human manganese superoxide dismutase, *J. Biol. Chem.* **274**, 24457-60.

Hearn, A. S., Stroupe, M. E., Cabelli, D. E., Lepock, J. R., Tainer, J. A., Nick, H. S., Silverman, D. N. (2001) Kinetic Analysis of Product Inhibition in Human Manganese Superoxide Dismutase. *Biochemistry* **40,** 12051-12058.

Hsieh, Y., Guan, Y., Tu, C., Bratt, P. J., Angerhofer, A., Lepock, J. R., Hickey, M. J., Tainer, J. A., Nick, H. S., Silverman, D. N. (1998) Probing the active site of human manganese superoxide dismutase: the role of glutamine 143, *Biochemistry* **37**, 4731-9.

Hsu, J. L., Hsieh, Y., Tu, C., O'Connor, D., Nick, H. S., Silverman, D. N. (1996) Catalytic properties of human manganese superoxide dismutase, *J. Biol. Chem.* **271**, 17687-91.

Hughes, M. N. and Nicklin, H.G. (1968) Part I. Kinetics of Decomposition of Pernitrous Acid. *J. Chem. Soc. (A)*, **2**, 450-452.

Hull, W. E. and Sykes, B. D. (1975) Dipolar nuclear spin relaxation of ^{19}F in multispin systems. Application to ^{19}F labeled proteins. *J. Chem. Phys.* **63**, 867-880.

Hull, W. E. and Sykes, B. D. (1975) Fluorotyrosine alkaline phosphatase – internal mobility of individual tyrosines and role of chemical shift anisotropy as a F-19 nuclear spin relaxation mechanism in proteins. *J. Mol. Biol.* **98**, 121-153.

Hunter, T., Ikebukuro, K., Bannister, W. H., Bannister, J. V., Hunter, G. J. (1997) The conserved residue tyrosine 34 is essential for maximal activity of iron-superoxide dismutase from Escherichia coli. *Biochemistry* **36**, 4925-4933.

Ischiropoulos, H. and Beckman, J.S. (2003) Oxidative stress and nitration in neurodegeneration: cause, effect, or association? *J. Clin. Invest.* **111**, 163–169.

Ischiropoulos, H., Zhu, L., Chen, J., Tsai, M., Martin, J. C., Smith, C. D., Beckman, J. S. (1992) Peroxynitrite-mediated tyrosine nitration catalyzed by superoxide dismutase. *Arch. Biochem. Biophys.* **298**, 431-437.

Jeffrey, G. A. (1997) An Introduction to Hydrogen Bonding, Oxford Press, Oxford.

Jones, T. A., Zou, J. -Y., Cowan, S. W., & Kjeldgaard, M. (1991) Improved methods for building protein models in electron density maps and the location of errors in these models. *Acta Cryst*. **A47**, 110-119.

Jude, K. M., Wright, S. K., Tu, C. K., Silverman, D. N., Viola, R. E. and Christianson, D. W. (2002) Crystal Structure of F65A/Y131C-methylimidazole Carbonic Anhydrase V Reveals Architectural Features of an Engineered Proton Shuttle. *Biochemistry* **41**, 2485-2491.

Kalra, J., and Prasad, K. (1994) Oxygen free radicals and cardiac depression, *Clin. Biochem.* **27**, 163-8.

Keele, B. B., Jr., McCord, J. M., and Fridovich, I. (1971) Further characterization of bovine superoxide dismutase and its isolation from bovine heart, *J. Biol. Chem.* **246**, 2875-80.

Laskowski, R.A., MacArthur, M.W., Moss, D.S. and Thornton, J. M. (1993) PROCHECK - a program to check the stereochemical quality of protein structures. *J. Appl. Cryst*. **26**, 283-291.

Leveque, V. J., Stroupe, M. E., Lepock, J. R., Cabelli, D. E., Tainer, J. A., Nick, H. S., and Silverman, D. N. (2000) Multiple replacements of glutamine 143 in human manganese superoxide dismutase: effects on structure, stability, and catalysis, *Biochemistry* **39**, 7131-7.

Leveque, V. J.-P., Vance, C.K., Nick, H.S., Silverman, D. N. (2001) Redox Properties of Human Manganese Superoxide Dismutase and Active-Site Mutants. *Biochemistry* **40,** 10586-10591.

Lymar, S. V., Jiang, Q., Hurst ,J.K. (1996) Mechanism of carbon dioxide-catalyzed oxidation of tyrosine by peroxynitrite. *Biochemistry* **35**:7855-7861.

MacMillan-Crow L. A., Crow, J. P., Kerby, J. D., Beckman, J. S., Thompson, J.A. (1996) Nitration and inactivation of manganese superoxide dismutase in chronic rejection of human renal allografts. *Proc. Nat. Acad. Sci.* USA **93,** 11853-11858.

MacMillan-Crow, L. A. and Thompson, J. A. (1999) Tyrosine modifications and inactivation of active site manganese superoxide dismutase mutant (Y34F) by peroxynitrite. *Arch. Biochem. Biophys*. **366**, 82-88.

MacMillan-Crow, L.A., Crow, J. P., Thompson J. A. (1998) Peroxynitrite-mediated inactivation of manganese superoxide dismutase involves nitration and oxidation of critical tyrosine residues. *Biochemistry* **37**, 1613-1622.

Maliekal, J., Karapetian, A., Vance, C., Yikilmaz, E., Wu, Q., Jackson, T., Brunold, T. C., Spiro, T. G., and Miller, A. F. (2002) Comparison and contrasts between the active site PKs of Mn-superoxide dismutase and those of Fe-superoxide dismutase, *J. Am. Chem. Soc.* **124**, 15064-75.

Marklund S.L., (1982) Human copper-containing superoxide dismutase of high molecular weight. *Proc. Natl. Acad. Sci. U S A.* **79,** 7634-8.

McAdam, M. E., Fox, R. A., Lavelle, F., and Fielden, E. M. (1977) A pulse-radiolysis study of the manganese-containing superoxide dismutase from Bacillus stearothermophilus. A kinetic model for the enzyme action, *Biochem. J.* **165**, 71-9.

McCord, J. M., and Fridovich, I. (1968) The reduction of cytochrome c by milk xanthine oxidase, *J. Biol. Chem.* **243**, 5753-60.

McCord, J. M., and Fridovich, I. (1969) Superoxide dismutase. An enzymic function for erythrocuprein (hemocuprein), *J. Biol. Chem.* **244**, 6049-55.

McPherson, A. (1982) *Preperation and analysis of protein crystals*. New York: Wiley and Sons.

Miller, A. F. (2004) Superoxide dismutases: active sites that save, but a protein that kills, *Curr. Opin. Chem. Biol.* **8**, 162-8.

Miller, A.-F., Padmakumar, K., Sorkin, D. L., Karapetian, A., Vance, C. K. (2003) Proton-coupled electron transfer in Fe-superoxide dismutase and Mn-superoxide dismutase. *J. Inorg. Biochem.* **93**, 71-83.

Mizuno, K., Whittaker, M. M., Bachinger, H. P., Whittaker, J. W. (2004) Calorimetric studies on the tight binding metal interactions of Escherichia coli manganese superoxide dismutase, *J. Biol. Chem.* ***279***, 27339-44.

Otwinowski, Z. a. M., W. (1997) Processing of X-ray diffraction data collected in Oscillation mode, *Methods Enzymol.* **276**, 307-326.

Purrello, M, Di Pietro, C, Ragusa, M, Pulvirenti, A, Giugno, R, Pietro, VD, Emmanuele, G, Travali, S, Scalia, M., Ferro, A. (2005) In vitro and in silico cloning of Xenopus laevis SOD2 cDNA and its phylogenetic analysis *DNA Cell Bio.*. **24**, 111-116.

Quijano, C., Hernandez-Saavedra, D., Castro, L., McCord, J. M., Freeman, B.A., Radi, R. (2001) Reaction of peroxynitrite with Mn-superoxide dismutase. Role of the metal center in decomposition kinetics and nitration. *J. Biol. Chem.* **276**, 11631-11638.

Quint, P., Reutzel, R., Mikulski, R., McKenna, R., Silverman, D. (2005) Crystal structure of nitrated human manganese superoxide dismutase: mechanism of inactivation, *Free Radic. Biol. Med.* **40**, 453-458.

Quint, P.S., Ayala, I., Busby, S. A., Chalmers, M. J., Griffin, P. R., Rocca, J., Nick, H. S., Silverman, D. N., (in press) Structural mobility in human manganese superoxide dismutase, *Biochemsitry*.

Rabini, J., Nielson, S. O. (1969) Absorption specrum and decay kinetics of $O_2^{\cdot-}$ and HO_2 in aqueous solutions by pulse radiolysis, *J. Phys. Chem***73**, 3736-3744.

Radi, R. (2004) Nitric oxide, oxidants, and protein tyrosine nitration. *Proc. Nat. Acad. Sci.* USA **101**, 4003-4008.

Radi, R., Cassina, A., Hodara, R., Quijano, C., Castro, L. (2002) Peroxynitrite reactions and formation in mitochondria. *Free Rad. Biol. and Med.* **33**, 1451-1464.

Ren, X., Bhatt, D., Perry, J. J. P., Tainer, J. A., Cabelli, D. E., and Silverman, D. N. (in press) Kinetic and structural characterization of human MnSOD containing 3-fluorotyrosine. *J. Molec. Structure*.

Santos, C. X., Bonini, M. G., and Augusto, O. (2000) Role of the carbonate radical anion in tyrosine nitration and hydroxylation by peroxynitrite, *Arch. Biochem. Biophys.* **377**, 146-52.

Schuettelkopf, A. W., van Aalten, D. M. F. (2004) PRODRG - a tool for high-throughput crystallography of protein-ligand complexes. *Acta Crystallographica* **D60**, 1355-1363.

Schwarz, H. (1981) Free radicals generated by radiolysis of aqueous solutions, *Journal of Chemical Education* ***58***, 101-105.

Shishehbor, M. H., Aviles, R. J., Brennan, M. L., Fu, X., Goormastic, M., Pearce, G. L., Gokce, N., Keaney, J. F. Jr, Penn, M. S., Sprecher, D. L., Vita, J. A., Hazen, S. L. (2003) Association of nitrotyrosine levels with cardiovascular disease and modulation by statin therapy. *JAMA* **289**, 1675-80.

Silverman, D.N. and Nick, H. S. (2002) Catalytic pathway of manganese superoxide dismutase by direct observation of superoxide. *Methods Enzymol.* **349**, 61-74.

Sines, J., Allison, S.A., Wierzbicki, A. and McCammon, J.A.. (1990) Brownian Dynamics Simulation of the Superoxide-Superoxide Dismutase Reaction: Iron and Manganese Enzymes. *J. Phys. Chem*. **94**, 959-961.

Slykhouse, T. O., and Fee, J. A. (1976) Physical and chemical studies on bacterial superoxide dismutases. Purification and some anion binding properties of the iron-containing protein of Escherichia coli B, *J. Biol. Chem.* **251**, 5472-5477.

Sorkin, D. L., Duong, D. K., Miller A. F. (1997) Mutation of tyrosine 34 to phenylalanine eliminates the active site pK of reduced iron-containing superoxide dismutase. *Biochemistry* **36**, 8202-9208.

Soulere, L., Claparols, C., Perie, J., Hoffmann, P. (2001) Peroxynitrite-induced nitration of tyrosine-34 does not inhibit Escherichia coli iron superoxide dismutase. *Biochem. J.* **360**, 563-567.

Stallings W. C., Metzger, A. L., Pattridge K. A., Fee J. A., Ludwig M. L. (1991) Structure-function relationships in iron and manganese superoxide dismutases. *Free Radical Res. Commun.* **12-13**, 259-268.

Tu, C., Quint, P., and Silverman, D. N. (2005) Exchange of (18)O in the reaction of peroxynitrite with CO(2), *Free Radic. Biol. Med.* **38**, 93-97.

Vance, C. K., Miller, A. F. (1998) Spectroscopic comparisons of the pH dependencies of Fe-substituted (Mn)superoxide dismutase and Fe-superoxide dismutase. *Biochemistry* **37**, 5518-5527.

Wagner, U. G., Pattridge, K. A., Ludwig, M. L., Stallings, W. C., Werber, M. M., Oefner, C., Frolow, F., and Sussman, J. L. (1993) Comparison of the crystal structures of genetically engineered human manganese superoxide dismutase and manganese superoxide dismutase from Thermus thermophilus: differences in dimer-dimer interaction, *Protein Sci. **2***, 814-825.

Weisiger, R. A., and Fridovich, I. (1973) Mitochondrial superoxide simutase. Site of synthesis and intramitochondrial localization, *J. Biol. Chem.* **248**, 4793-4796.

Whittaker, M. M. and Whittaker J. W. (1997) Mutagenesis of a proton linkage pathway in Escherichia coli manganese superoxide dismutase. *Biochemistry* **36**, 8923-8931.

Whittaker, M. M. and Whittaker, J. W. (1998) A glutamate bridge is essential for dimer stability and metal selectivity in manganese superoxide dismutase. *J. Biol. Chem.* **273**, 22188-22193.

Whittaker, M. M., and Whittaker, J. W. (2000) Recombinant superoxide dismutase from a hyperthermophilic archaeon, Pyrobaculum aerophilium, *J. Biol. Inorg. Chem.* ***5***, 402-408.

Wintjens, R., Noel, C. May, A. C. W., Gerbod, D., Dufernez, F., Caparon, M., Viscogliosi, E. and Rooman, M. (2004) Specificity and phenetic relationships of Fe- and Mn-containing superoxide dismutases on the basis of structure and sequence. *J. Biol. Chem.* ***279***, 9248-9254.

Yamakura, F., Taka, H., Fujimura, T., Murayama, K. (1998) Inactivation of human manganese-superoxide dismutase by peroxynitrite is caused by exclusive nitration of tyrosine 34 to 3-nitrotyrosine. *J. Biol. Chem.* **273**, 14085-14089.

BIOGRAPHICAL SKETCH

In 1995, Patrick Quint received his high school diploma from Rocky Mountain High School in Ft. Collins, CO, and then moved to St. Paul, MN, where he attended Macalester College. Upon receipt of his BA in biology, he worked at 3M for two years before attending graduate school at University of Florida. After successfully defending his dissertation, he will receive a post-doctoral appointment in the lab of Dr. Bob Bergen at the proteomics division at Mayo Clinic in Rochester, MN.